Spray droplets under turbulent conditions

Rouault, M.; Larsen, Søren Ejling

Publication date:
1990

Document Version
Publisher's PDF, also known as Version of record

Risø-M-2847

Spray Droplets under Turbulent Conditions

Mathieu Rouault and Søren E. Larsen

Risø National Laboratory, DK-4000 Roskilde, Denmark
February 1990

Abstract In the frame of the international cooperative program HEXIST, in parallel to the experiments conducted in IMST Large Air-Sea Interaction Simulation Tunnel, we have developed a numerical model of turbulent transport and evaporation of a population of droplets ejected by bursting bubbles at the water surface. This numerical model considers fresh water droplets from 10 to 100 microns radius (jet drops), in a fully developed turbulent boundary layer or any constant flux layer, with no surface waves. The droplet population is separated in 20 categories according to their size, and each category is considered as a scalar field transported along with the scalar fields of temperature and water vapor concentration by turbulence. Theses fields are interacting through source-sink functions, representing droplets shrinking and water vapour production due to droplet evaporation. Droplet surface production and deposition processes, and inertial and gravitational effects are explicitly modeled. Droplet diffusion by air turbulence is modeled by a K diffusivity. The model has been fitted to the conditions of CLUSE-HEXIST 3, the large experiment that has been conducted by HEXIST participants in the IMST tunnel in May-June 1988.

After a description of the model and numerical method we will make some comparisons with the experiment CLUSE-HEXIST 3. Then we will study some cases in a idealistic constant flux boundary layer in different humidity and wind configurations. Finally, we will compare our ejected drop flux to that found by Bortkovskii (1987) which will be used in different configurations.

ISBN 87-550-1608-1
ISSN 0418-6435

Grafisk Service Risø 1990

Contents

1 Introduction

In heat and moisture exchanges and above all mass transfer between atmosphere and ocean the importance of spray droplets is really significant under turbulent conditions. Parallel to the experimental research of the HEXIST program, a numerical code has been made in order to model the diffusion and evaporation of spray droplets in a turbulent field. This field is the boundary layer over the water surface in the IMST large air-sea interaction simulation tunnel. Our attention is only drawn to the jet droplets generated by bursting bubbles.

2 Formulation of the CLUSE model

2.1 The equations

2.1.1 The hypothesis

a The fluid is assumed to be incompressible.

b The Coriolis force is negligible.

c There is no chemical reaction.

d We use the Boussinesq approximation.

e We suppose that the droplets are spherical and do not split by atomisation or by shocks.

f We assume that the number of droplets in the domain of study is conserved.

g We are in a fully developed boundary layer and apply the classical homogeneity hypothesis. The flux constant hypothesis used in all the domain is very important because that conditions all the turbulence effect.

h We also hypothesize that the density of droplets is too small to have any influence on the dynamics of air.

i We only take into account the jet drops and are using the relationships given by Blanchard (1963) for ejecting heights and drop diameters.

2.1.2 The instantaneous equations

We consider the fluid as a multiphase mixture of $N+2$ components: dry air with a ρ_a-concentration, water vapor with a ρ_v−concentration, and N droplet categories of radius $r_n, n = 1, \ldots, N$ with a ρ_n-concentration. Category n with nominal radius, r_n, includes all droplets of radius defined by:

$$r_n - \delta_{rn}/2 < r < r_n + \delta_{rn}/2 \tag{1}$$

The instantaneous equations of mass conservation of the $N+2$-components are:

$$\frac{\partial \rho_\gamma}{\partial t} + \frac{\partial (\rho_\gamma V_{\gamma j})}{\partial x_j} = S_\gamma \ , \ \gamma = a, v, n, \ n = 1, \ldots, N \tag{2}$$

where $V_\gamma j$ is the velocity of the component γ and S_γ are source terms due only to the droplets evaporation. The source functions are related by:

$$\begin{cases} S_a = 0 \\ S_v + \sum_{n=1}^{N} \quad S_n = 0 \end{cases} \tag{3}$$

We now introduce in Eq. (2) the slip velocity:

$$\vec{\Delta}_\gamma = \vec{V}_\gamma - \vec{V} \tag{4}$$

where $\vec{V}$ is the velocity of the mixture. The budget equations (2) are now defined by:

$$\begin{aligned}
\frac{\partial \rho_n}{\partial t} + \frac{\partial \left(\rho_n \Delta_{n_j} + \rho_n V_j\right)}{\partial x_J} &= S_n \\
\frac{\partial \rho_v}{\partial t} + \frac{\partial \left(\rho_v \Delta_{v_j} + \rho_v V_j\right)}{\partial x_J} &= -\sum_1^N S_n \\
\frac{\partial \rho_a}{\partial t} + \frac{\partial \left(\rho_a \Delta_{a_j} + \rho_a V_j\right)}{\partial x_j} &= 0 \quad .
\end{aligned} \tag{5}$$

2.1.3 The average equations

Every instantaneous quantity characterizing the turbulent flow can be decomposed into a mean $\bar{\Phi}$ and a fluctuating part Φ' (with $\overline{\Phi'} = 0$):

$$\Phi = \bar{\Phi} + \Phi' \tag{6}$$

Using the hypothesis, h, (section 2.1.1), we assume that the vertical velocity of dry air, W_a, and the water vapor, W_v, are equal to the fluid velocity, W:

$$W_a = W_v = W \quad .$$

We can also use the homogeneity hypothesis, g (section 2.1.1) which allows us to write:

$$\frac{\partial \bar{\Phi}}{\partial x} = \frac{\partial \bar{\Phi}}{\partial y} = 0 \tag{7}$$

$$\bar{W} = 0 \tag{8}$$

so, $\overline{W_a} = 0$, $\overline{W_v} = 0$, $\overline{W} = 0$, and $\overline{\Delta_{nz}} = \overline{W_n}$ where $\overline{\Delta_{nz}}$ is the mean vertical component of the slip velocity and $\overline{W_n}$ the mean droplet-velocity component of category n.

After introduction of the decomposition, Eq. (6), in Eq. (5) we average these equations. Taking the preceding hypothesis into account and neglecting the molecular diffusivity, we can now write the mean continuity equation for the $N+2$ components:

$$\underbrace{\frac{\partial \overline{\rho_n}}{\partial t}}_{1} = -\underbrace{\frac{\partial \left(\overline{\rho_n' w'}\right)}{\partial z}}_{2} - \underbrace{\frac{\partial \left(\overline{\rho_n' \Delta_{nz}'}\right)}{\partial z}}_{3} - \underbrace{\frac{\partial \left(\overline{\rho_n}\,\overline{W_n}\right)}{\partial z}}_{4} + \underbrace{S_n}_{5} \tag{9}$$

$$\underbrace{\frac{\partial \bar{\rho}_v}{\partial t}}_{1} = -\underbrace{\frac{\partial \left(\overline{\rho_v' w'}\right)}{\partial z}}_{2} - \underbrace{\sum_1^N S_n}_{6} \tag{10}$$

where the following terms appear:

1 time variation (nul in stationary state)

2 turbulence diffusion

3 counter-diffusion due to the droplet inertia

4 macroscopic flux due to the droplet dynamic (ejection and fall on gravity effect)

5,6 Source term due to the droplet evaporation. Because of these two terms we have to write a equation for the sensible heat, as the evaporation rate of a droplet is of course related to the sensible heat, which changes during the evaporation. During evaporation, the sensible heat decreases:

$$\frac{\partial \bar{T}}{\partial t} = -\frac{\partial\left(\overline{T w'}\right)}{\partial z} + \frac{L_w}{\rho_a\, Cp} \sum_1^N S_n \tag{11}$$

Term 3 in Eq. 9 could be modelled by a counter-diffusion term in order to reduce the turbulence diffusion as a function of the droplet radius and the intensity of the turbulence. This term has been modelled as follows:

$$\frac{\partial\left(\overline{\rho'_n}\,\Delta'_{n_s}\right)}{\partial z} = -\frac{\partial}{\partial z}\left(K'_n \frac{\partial \overline{\rho_n}}{\partial z}\right) \tag{12}$$

where

$$K'_n = K_n \left(C_2 \frac{V_f^2}{1.56\, u_*^2}\right)^{-1} \tag{13}$$

where V_f is the final fall velocity calculated in section A.3 and u_* is the velocity friction. The total diffusion is modelled by:

$$\frac{\partial}{\partial z}\left((K_n + K'_n)\frac{\partial \overline{\rho_n}}{\partial z}\right) \quad . \tag{14}$$

Unfortunately, we cannot study and valid this term because of the lack of data concerning the ejected drop flux and the deposition velocities of the droplets under turbulent conditions. We suppose that this term is small compared to the turbulence diffusion (term 2) and the gravitational effect (term 4). Consequently, we will neglect this term, but in section 3.3 we will study how it has been modelled and what the effects are.

Term 4 in Eq. 9 obliges us to add to the system one momentum equation for each droplet category. In effect, the ejection velocity of the droplets is important, causing the droplets to go up to 1–20 cm which is not negligible compared to the study domain (about 1 m). Furthermore, we cannot neglect the effect of gravity for the jet droplets which are big enough to have an important fall velocity.

However, we have to produce a model of this term because we do not know the ejection heights and the fall velocities under turbulent conditions. Some authors, Edson (1989); Ling et al. (1980), do it with:

$$-\frac{\partial\left(\bar{\rho}_n \bar{W}_n\right)}{\partial z} = -\frac{\partial\left(\bar{\rho}_n \bar{V}_g\right)}{\partial z} \tag{15}$$

where V_g is a constant velocity, usually the Stokes velocity, (Eq. 101), the terminal velocity (Eq. 100), or a fraction of V_s or V_l.

In our study we produce a model of term 4, using a relaxation term:

$$\frac{\bar{\rho}_n - \rho_{on}}{C_1\, T_{vn}} \tag{16}$$

where ρ_{on} is the value of ρ_n under a non-turbulent condition, T_{vn} is the suspension or flight time of a droplet under non-turbulent conditions. ρ_{on} ,and T_{vn} are calculated in section A.3. The modelling of term 4 and its effects will be discussed in section 2.3.

2.1.4 The closure equations

$\frac{\partial\left(\overline{\rho'_n w'}\right)}{\partial z}$, $\frac{\partial\left(\overline{\rho'_v w'}\right)}{\partial z}$, $\frac{\partial\left(\overline{T' w'}\right)}{\partial z}$, is the classical eddy diffusion term and is related to the mean quantity gradients by the exchange coefficients:

$$\overline{\rho'_n w'} = -K_n \frac{\partial \overline{\rho_n}}{\partial z} \tag{17}$$

$$\overline{\rho'_v w'} = -K_v \frac{\partial \overline{\rho_v}}{\partial z} \tag{18}$$

$$\overline{T'w'} = -K_t \frac{\partial \overline{T}}{\partial z} \tag{19}$$

with

$$\text{For the temperature : } K_t = \frac{\sigma_t}{\mathrm{Pr}_t} \tag{20}$$

$$\text{For the water vapor : } K_v = \frac{\sigma_t}{\mathrm{Sc}_t} \tag{21}$$

$$\text{For the droplets : } \quad K_n = \frac{\sigma_t}{\mathrm{Sc}_{tn}} \tag{22}$$

where σ_t is the eddy viscosity, Pr_t and Sc_t are the Prandtl and Schmidt turbulence numbers. We use:

$$\mathrm{Pr}_t = \mathrm{Sc}_t = 0.74 \quad . \tag{23}$$

In the absence of experimental data concerning Sc_{tn} (which can be called Schmidt numbers of turbulence in the n-category droplets), we assume as in Melville and Bray (1979) that $Sc_{t_n} = Sc_t = 0.74$.

In the boundary layer condition, the eddy viscosity is defined as:

$$\sigma_t = \kappa u_* z \tag{24}$$

where κ is the von Karman constant ($\kappa = 0.4$) and u_* is a friction velocity characteristic of the flow. With the flux constant hypothesis, u_* is constant in all domains and given by:

$$u_* = \left(\tfrac{1}{2} C_f U_\infty^2\right)^{1/2} \tag{25}$$

where U_∞ is a reference velocity and C_f a friction coefficient, input data of the model. The system of Eqs. 9, 10, 11 is now closed and can be written:

$$\frac{\partial \overline{\rho}_n}{\partial t} = \frac{\partial}{\partial z}\left(K_n \frac{\partial \overline{\rho}_n}{\partial z}\right) - \frac{(\overline{\rho}_n - \rho_{on})}{C_1 \cdot T_{vn}} + S_n \tag{26}$$

$$\frac{\partial \overline{\rho}_v}{\partial t} = \frac{\partial}{\partial z}\left(K_v \frac{\partial \overline{\rho}_v}{\partial z}\right) - \sum_1^N S_n \tag{27}$$

$$\frac{\partial \overline{T}}{\partial t} = \frac{\partial}{\partial z}\left(K_t \frac{\partial \overline{T}}{\partial z}\right) + \frac{L_w}{\rho_a C_p} \sum_1^N S_n \tag{28}$$

2.2 The numerical method

2.2.1 Numerical modeling of the equations

The code used in this study was elaborated from a Roland Shiestel code used for the numerical predetermination of stationary flow. This code calculates the diffusion of a quantity Φ, whose equation is:

$$\frac{\partial}{\partial z}\left(K \frac{\partial \overline{\Phi}}{\partial z}\right) + S_\Phi = 0 \tag{29}$$

$$S_\Phi = S_U + \Phi\, S_p \tag{30}$$

The resolution of this stationary equation is found by iteration, the solution is the time limit of the nonstationary equation:

$$\frac{\partial \overline{\Phi}}{\partial t} = \frac{\partial}{\partial z}\left(K \frac{\partial \overline{\Phi}}{\partial z}\right) + S_\Phi \tag{31}$$

We use this process for a iterative solution of the non-linearities, and are not interested in the transitory solution.

We employ the finite volumes method (micro-integral method) derived from the Patankar and Spalding study (1970). S_p has to be negative to solve the equations.

The domain of the study is one-dimensional along the boundary vertical axis. The grid space step Δz is arbitrarily fixed in order to have narrow steps where the variables vary a lot. To do so, we use a logarithmic distribution for the discrete point $z(i)$:

$$z(i) = z(i-1) + \Delta z(i) \tag{32}$$

with

$$\Delta z(i) = \chi\, \Delta z(i-1) \tag{33}$$

where $\chi > 1$. Because T and ρ_v vary rapidly with height near the water surface, we must have a lot of discrete points in the lower layer. Thus we have to use a minimum value of 1.06 for χ. If χ is too large, we have an insufficient number of points in the rest of the layer.

The domain is divided into domains of control D_i surrounding each grid level $z(i)$. The method consists of integrating the equations in each domain of control. The discrete equations have the following form:

$$\Phi_i = A\Phi_{i+1} + B\Phi_{i-1} + C \tag{34}$$

In this relation the A, B, and C coefficients are calculated in a specific way at the upper and lower boundary to respect the boundary conditions. The resolution of the system is made with the tridiagonal algorithm.

2.2.2 The initial conditions

The initial conditions are not very important because we are not interested in the transitory solution, but the closer the initial profile is to the solution, the fewer the iterations required by the numerical method. We suppose that the variable has the same values as in the non-perturbed boundary layer:

$$\rho_n(z) = 0 \tag{35}$$

Initially, T and ρ_v have the logarithmic profiles which characterize the boundary layer with the idealistic flux constant hypothesis (cf section 4.1).

2.2.3 The boundary conditions

Upper boundary. The droplet conditions are defined in order to conserve the total number of droplets throughout the domain:

$$\rho_n(z_{\text{sup}}) = 0 \quad , \tag{36}$$

but some significant numerical experiments have shown that we have the same results with the Neuman condition:

$$\left(\frac{d\bar{\rho}_n}{dz}\right)_{z=z_{\text{sup}}} = 0 \quad . \tag{37}$$

For T and ρ_v we use the Dirichlet conditions:

$$T(z_{\text{sup}}) = T_{\text{sup}} \tag{38}$$

$$\rho_v\,(z_{\text{sup}}) = \rho_{v\,\text{sup}} \tag{39}$$

Lower boundary. The temperature value at $z = z_{inf} = 1.5\,10^{-4}$ m is the water surface temperature, and the water vapor concentration is the saturating water vapor concentration at the water surface temperature.

$$\bar{T}(z_{inf}) = T_{surf} \tag{40}$$

$$\bar{\rho}_v(z_{inf}) = \rho_{v_{surf}} \tag{41}$$

The concentration of category n, $\overline{\rho_n}(z_{inf})$, is the sum of the ejected concentration, ρ_{ne}, and the deposition concentration, ρ_{nf}:

$$\overline{\rho_n}(z_{inf}) = \rho_{ne} + \rho_{nf} \tag{42}$$

The surface flux, $F(z_{inf})$ is the sum of the ejection and deposition flux:

$$F(z_{inf}) = \rho_{ne} W_{ne} + \rho_{nf} W_{nf} \tag{43}$$

where W_{ne} is modelled by the ejection velocity and W_{nf} by the final fall velocity $-V_f$, both calculated in section A3 under non-turbulent conditions. If we integrate the $\bar{\rho}_n$ equation (9) over the entire height of the boundary layer when $\partial\overline{\rho_n}/\partial t = 0$, it appears that

$$\int_{z_{inf}}^{z_{sup}} S_n \, dz = -F(z_{inf}) \tag{44}$$

where S_n is the source term 5 of Eq. 9. Consequently, we deduce from Eqs. (42, 43, and 44):

$$\bar{\rho}_n(z_{inf}) = \rho_{ne} - \frac{\int_{z_{inf}}^{z_{sup}} S_n \, dz + \rho_{ne} W_{ne}}{W_{nf}} \tag{45}$$

2.3 Relaxation coefficient study

The relaxation term: $(\bar{\rho}_n - \rho_{on}) / (C_1.T_{vn})$ (Eq. 16) is introduced to take into account the dynamic of the droplets. Under turbulent conditions the droplets are ejected to an unknown height and fall down at an unknown fall velocity. Now let us see how the relaxation term can take into account the ejection and fall of the droplets.

a Subtracting this term in Eq. (9) conducts to add a source term

$$\rho_{on} / (C_1.T_{vn})$$

which is null above the ejection height. Without this term the calculation would operate by the turbulence diffusion from the lower boundary, ($z = 0$) as the temperature or the water vapor concentration.

b In a non-evaporative case and when the turbulence decreases ($u_* \rightarrow 0$) Eq. (9) becomes:

$$\frac{1}{C_1.T_{vn}} (\bar{\rho}_n - \rho_{on}) = 0 \tag{46}$$

such that $\bar{\rho}_n \rightarrow \rho_{on}$, which is the solution in non-turbulent conditions.

c the term $\overline{\rho_n} / (C_1.T_{vn})$ is substracted from Eq. 9. This term models the fall of the droplets as a sink term for the ρ_{on} equation throughout the domain.

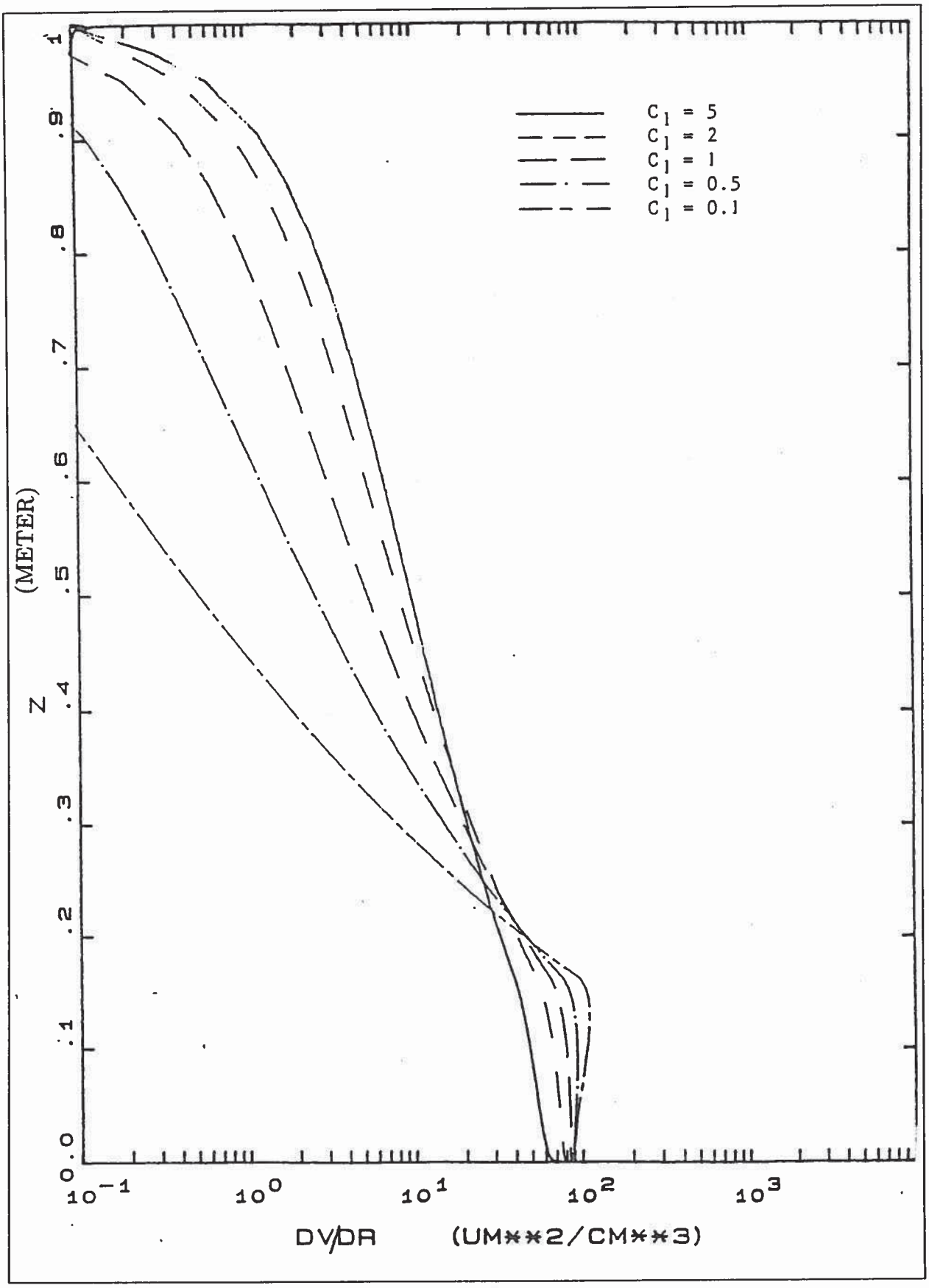

Figure 1a. Influence of the relaxation term on vertical volumic concentration by radius increment, dV/dr for the 100 μm category for different C_1 values; $u_* = 0.36$, $\delta_{rn} = 5$ microns.

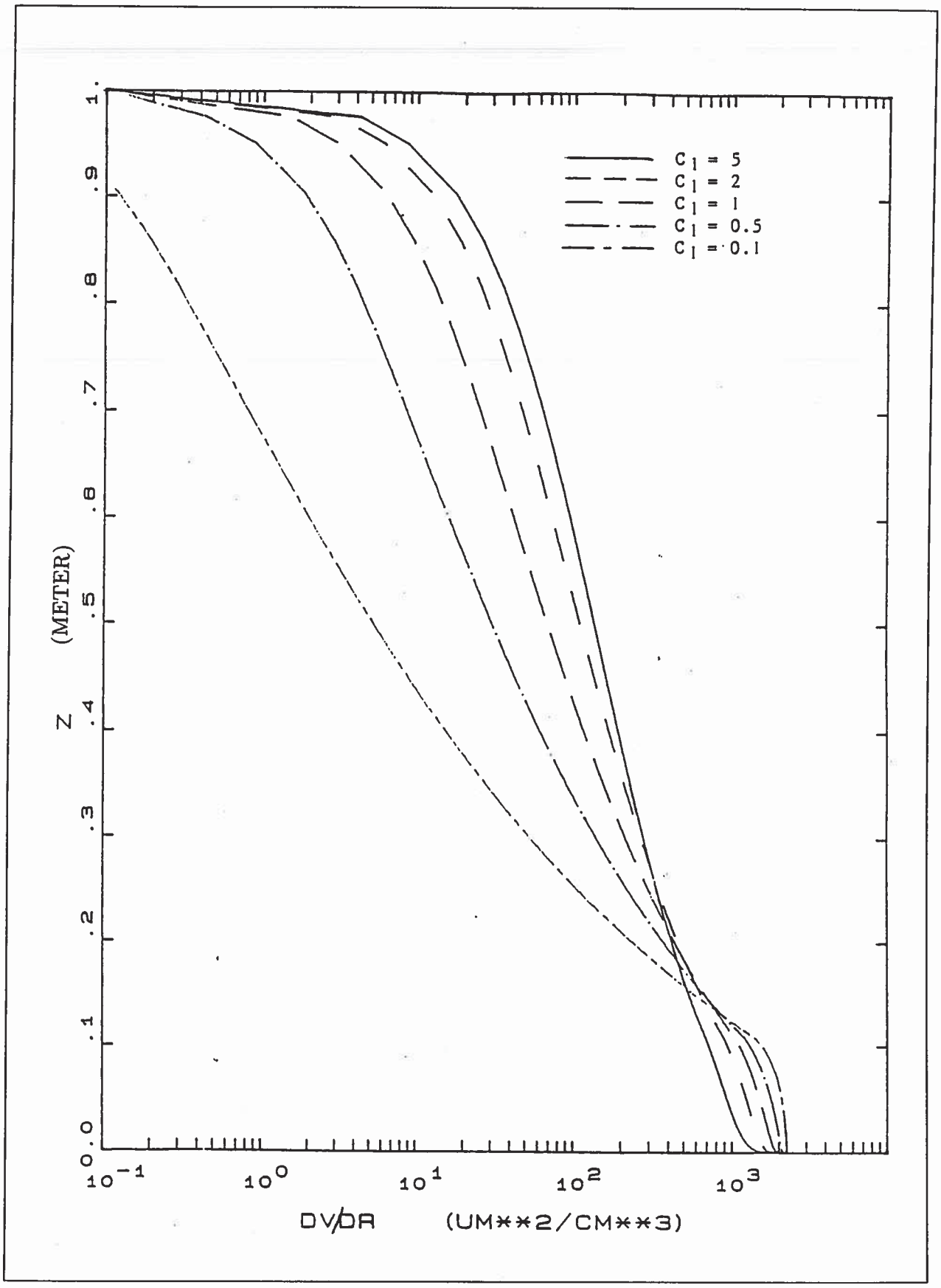

Figure 1b. Influence of the relaxation term on vertical volumic concentration by radius increment, dV/dr for the 50 μm category for different C_1 values; $u_* = 0.36$, $\delta_{rn} = 5$ microns.

In Figs. 1a and 1b we present the variation of vertical volumic concentration by radius increment, dV/dr with C_1 ($C_1 = 5, 2, 1, 0.5, 0.1$) for two droplet categories: 100 μm (Fig. 1a) and 50 μm (Fig. 1b) for a 10.5 m/s wind speed ($u_* = 0.36$) in non-evaporative conditions. δ_{rn}=5 μm for all the categories.

The height of the domain is 1 meter. We use an ejected drop flux function deduced from the CLUSE-HEXIST3 experiment, the model (section 3) and the ejection height given by Blanchard, 1963 (11 cm for the 50 μm category and 16 cm for the 100 μm category).

We suppose that the droplets appear at their ejection height, supposing that the droplets immediately reach their final velocity, we can write:

$$\rho_{on} = \frac{\rho_{ne}\, w_{ne}}{V_f} \tag{47}$$

where V_f is the fall velocity calculated in Appendix and w_{ne} the ejection velocity of the n category droplets also calculated in Appendix A. These two hypotheses, which lead to the ρ_{on} calculation, will be discussed in the appendix A. In Figs. 1a and 1b we can distinguish two areas separated at a height close to the ejection height.

The effect of the relaxation term is to increase the concentration below and to decrease it above the ejection height; so we have modeled the increase by ejection and the decrease due to the gravity effect.

We notice that the smaller C_1, the more $\overline{\rho}_n \rightarrow \rho_{on}$, below the ejection heights while above the ejection height $\overline{\rho}_n / (C_1 . T_{vn})$ increases, and consequently the effect of droplet fall increases.

C_1 has been adjusted to 0.75 by comparing the calculations with the CLUSE-HEXIST3 experiment.

2.4 Modeling the source-sink term S_n

S_n is the source-sink term of the ρ_n Eq. (12) and results from the droplet evaporation. We assume the conservation number of droplets in the calculation domain. Thus, the totally evaporated droplets still exist with a null radius (correct in case of droplets with solid nuclei). This is the reason why we have the null droplet concentration hypothesis at the upper boundary which allows us to write the lower boundary condition for the droplets (section 2.2.3). The droplet number by radius increment, s_r, is a conservative quantity in the four-dimensional space $(x, y, z.r)$. In this space, the velocity componants are $(V_{rx}, V_{ry}, V_{rz}, \dot{r})$ where $\dot{r} = \mathrm{dr/dt}$. The s_r-equation of conservation is:

$$\frac{\partial s_r}{\partial t} + \frac{\partial (s_r\, V_{rj})}{\partial x_j} + \frac{\partial (s_r\, \dot{r})}{\partial r} = 0 \quad . \tag{48}$$

In the usual space (x, y, z), the ρ_r equation of conservation is:

$$\frac{\partial \rho_r}{\partial t} + \frac{\partial (\rho_r\, V_j)}{\partial x_j} = S(r) \tag{49}$$

where $S(r)$ is a source–sink term of the radius droplets, r due to evaporation. The mass concentration of a radius droplet, r, is:

$$\rho_r = \frac{4}{3}\, \pi\, r^3 \rho_w\, s_r \tag{50}$$

Thus, Eq. (49) can be written :

$$\frac{4}{3}\, \pi\, \rho_w \left(r^3 \frac{\partial s_r}{\partial t} + 3\, r^2\, s_r\, \dot{r} + r^3 \frac{\partial (s_r\, V_j)}{\partial x_j} \right) = S(r) \quad . \tag{51}$$

If we approximate V_{rx}, V_{ry}, and V_{rz} by Vx, Vy, and Vz, we can write with Eqs. (48) and (51):

$$\frac{4}{3}\,\pi\,\rho_w\left(3\,r^2\,s_r\,\dot{r}-r^3\frac{\partial\,(s_r\,\dot{r})}{\partial r}\right)=S(r) \tag{52}$$

Consequently,

$$\frac{4}{3}\,\pi\,\rho_w\left(3\,r^2\,s_r\,\dot{r}-r^3\,\dot{r}\frac{\partial s_r}{\partial r}-r^3\,s_r\,\frac{\partial\dot{r}}{\partial r}\right)=S(r)\quad . \tag{53}$$

Or, as a function of ρ_r

$$S(r)=6\,\rho_r\,\frac{\dot{r}}{r}-\dot{r}\frac{\partial\rho_r}{\partial r}-\rho_r\frac{\partial\dot{r}}{\partial r} \tag{54}$$

We have to model $\dot{r}$. The droplet evaporation rate is governed by the water vapor transfer between the droplet surface and the surrounding air. If the air and the droplet have different velocities, the transfer is increased due to ventilation of the droplet by renewed air. Beard and Prupacher (1971) model this effect in the evaporation rate formula by a "ventilation factor", f_r. For dm_r/dt, we can write the mass evaporation variation rate of a radius droplet, r:

$$\frac{dm_r}{dt}=\frac{-4\,\pi\,r\,f_r\,Dv\,(\rho_{vs}(Tp)\,Tp-\rho_v(z)\,T(z))}{\left(1-\frac{\rho_{vs}(Tp)+\rho_v(z)}{2\,\epsilon\,\rho_a}\right)\left(\frac{Tp+T(z)}{2}\right)} \tag{55}$$

where Dv is the water vapor diffusivity, ρ_{vs} is the saturating water vapor mass concentration, Tp is the droplet surface temperature, and $\epsilon=R'/Rv=0.611$. To determine Tp (Edson, 1987; Andreas, 1989) we have studied the Tp-variation with a heat transfer equation given by Prupacher and Klett (1978). Their calculations indicate that the heat transfer is much faster than the water vapor transfer. It appears that Tp tends quickly to the wet bulb temperature, Th. Thus, we assume that $Tp=Tw$. Th is found from the heat equilibrium equation:

$$\rho_a\,Cp\,Tw\;+\;Lw\,\rho_{vs}(Tw)\;=\;\rho_a\,Cp\,T\;+\;Lw\,\rho_v \tag{56}$$

Thus,

$$Tw\;=\;T-\frac{Lw}{Cp}\frac{\rho_{vs}(Tw)-\rho_v}{\rho_a} \tag{57}$$

and

$$Tw\;=\;T-\frac{Lw\,\epsilon}{Cp\,P}\,(e_{vs}\,(Tw)-e_v)\quad , \tag{58}$$

where $e_{vs}\,(Tw)$ is the saturating water vapor pressure, T the air temperature, and P the total pressure. We can determine Tw by successive approximation, but it is easier to calculate first e_{vs}. From equation 58 we can write:

$$e_{vs}=e_v+\frac{Cp\,P}{Lw\,\epsilon}\,(T-Tw\,(e_{vs})) \tag{59}$$

where $Tw(e_v)$ can be found from the formula given by Buck (1981):

$$Tw\,(e_v)=273.15+\frac{240.97\,\log(e_v/611.21)}{17.502-\log(e_v/611.21)} \tag{60}$$

e_v is in Pascal and T in Kelvin. To calculate $Tw\,(e_{vs})$ we start with $e_{vs}=e_v$ in equation 60 and carry back this value to equation 59. Then we calculate a first e_{vs}-value to be carried back to equation 60. We repeat this iteratively until the Tw and e_{vs}(Tw)- values converge. The relation:

$$\frac{dm_r}{dt}=4\,\pi\,\rho_w\,r^2\,\dot{r} \tag{61}$$

allows us to write the equation 55:

$$\dot{r}=-\frac{A}{r} \tag{62}$$

where

$$A = r f_r Dv \rho_w^{-1} (\rho_{vs}(Tw)Tp - \rho(z)T(z)) \times \left(1 - \frac{\rho_{vs}(Tp) + \rho_v(z)}{2\epsilon\rho_a}\right)^{-1} \left(\frac{Tp + T(z)}{2}\right)^{-1} \quad (64)$$

(65)

f_r is given by Beard and Prupacher (1971):

$$f_r = 0.78 + 0.308 N \quad for\ N < 1.4$$

$$f_r = 1 + 0.108 N^2 \quad for\ N > 1.4 \quad (66)$$

where $N = Sc_t^{1/3} Re(r)^{1/2}$. In the Re-calculation we use the fall velocity, V_f calculated in section A.3. With equation 62 we can write equation 54 as:

$$S(r) = -A\frac{6\rho_r}{r^2} + \frac{A}{r}\frac{\partial\rho_r}{\partial r} - A\frac{\rho_r}{r^2} \quad . \quad (67)$$

Thus

$$S(r) = -A\left(\frac{7\rho_r}{r^2} - \frac{1}{r}\frac{\partial\rho_r}{\partial r}\right) \quad . \quad (68)$$

This equation is written for identical radius droplets. For the category n with radius r_n, which include all radii between $r_n - \delta_{r_n}/2$ and $r_n + \delta_{r_n}/2$, we can approximate Sn if δ_{r_n} is small by:

$$Sn = -A\left(\frac{7\rho_{r_n}}{r_n^2} - \frac{1}{r_n}\frac{\partial\rho_{r_n}}{\partial r_n}\right) \quad . \quad (69)$$

We can then deduce the source–sink term of the temperature and water vapor equations, S_v and S_T:

$$S_v = -\sum_1^N S_n \quad (70)$$

$$S_T = +\frac{L_w}{\rho_a Cp}\sum_1^N S_n \quad (71)$$

3 Comparison of experiment calculation without evaporation

3.1 Introduction

The CLUSE model had to be compared with the experimental data of the experiment CLUSE–HEXIST 3 (de Leeuw, 1988) in order to adjust the C_1 constant and to verify the model hypothesis. Unfortunately, all the experimental results are unavailable, particularly the RISP and ROTOROD measurements.

The concentration measurements of the ejected droplet flux are not available. But because of the complexity of the physics phenomena involved and the technical difficulties of the measurements, a long time will be required before it is known. This lack of knowledge presents a problem for us because the ejected concentration is used in the lower boundary layer condition (section 2.2.3) and in the relaxing term Eq. (16). So we have to adjust ρ_{en} with an arbitrary value of C_1.

3.2 Ejected concentration adjustment

Under non-evaporative conditions, the ρ_n-equations are independent, but we present the results for the 19 droplet categories ($r_n = 10, 15, 20 \ldots, 100$ μm with $\delta_{r_n} = 5$ μm). We begin to adjust ρ_{en} with the high wind speed in the 19 May experiments where $u_{reference} = 11$ m/s.

The most important parameter for the turbulence effects is u_*. We use the values given by Jim Edson after the CLUSE-HEXIST3 experiments which confirm that the boundary layer is not a constant flux layer. Jim Edson has averaged the u_* calculated during the turbulence profile experiment. u_* is given by:

$$u_*(z) = u_*(z_{inf})\,(1 + (z/\lambda)^6)^{-1} \tag{71}$$

where

$$\lambda = 49 \qquad u_m > 500 \text{ cm/s} \tag{72}$$

$$\lambda = 1.57\,u_*(z_{inf}) + 13.7 \qquad u_m < 500 \text{ cm/s} \tag{73}$$

where $u_*(z = z_{inf}) = 0.045\,u_m$ and $u_m = u(z = 0.70)$ cm. These profiles have been done for the 7.5 m/s and 3.5 m/s cases but we extend it to 11 m/s.

Fortunately, some comparisons of calculations made with the u_*-constant and with u_* as a function of z have shown no important discrepancy for the vertical concentration profile between the two cases. But this is not the same for the temperature and water vapor concentration equations which are more dependent on the turbulence term. So in its current state, the CLUSE model cannot be compared with the CLUSE-HEXIST3 experiment in evaporative cases. Therefore, we will first examine some non-evaporative cases.

For the 19 May experiment, $u_* = 0.49$ ($u_\infty = 11$ m/s). We use $C_1 = 0.75$, and ρ_{en} is adjusted for each category until they match the 19 May measurement (file No. 26, Fig. 2c) made at $z = 37.6$ cm.

Then we compare the calculation with the other 19 May measurements made at different heights, (9.18 to 60.79 cm, Figs. 2a to 2e). We can see that the calculation underestimates the concentration in the lower part for radius > 40 μm. Above 40 cm the discrepancy increases with z.

We have also compared the calculation with the 20 May measurements (file Nos. 32 to 40) made with a lower wind speed $U_{reference} = 7.5$ m/s. We just changed the u_* value ($u_* = 0.36$, $u_\infty = 8$ m/s). We had the same underestimate in the lower part and a larger overestimate in the upper part than in the preceding calculation. The adjusted value of the ejected drop flux used in the preceding calculation is presented in Fig. 3.

From 23 May the experiments are made with 1/3 of the bubbler, but because the total bubbler efficiency is changed it is difficult to rely on the two bubble fluxes and consequently the two experimental serials. Thus, we have found the new ejected concentration ρ_{en} by adjusting with the 23 May measurement (file No. 66) with $u_* = 0.36$. The value of the ejected drop flux is presented in Fig. 3 and compared with the preceding ejected concentration. The two distributions are close to an apparently constant ratio (= 2) for a radius > to 30 μm.

We now compare the source function deduced from the 23 May experiment produced with one third of the bubblers with the source function found by Jim Edson (1989) by comparisons between his Lagrangian model and the CLUSE-HEXIST 3 experimental data. His source function is closer to the de Leeuw measurement as we can see in Fig. 4 except for the droplet with radius > 50 microns. Edson (1989) is of opinion that the measurements overestimate the size of the larger droplets and his source function is accurate. The underestimation of the CLUSE model source function for the droplets > 40 microns could be explained because we are

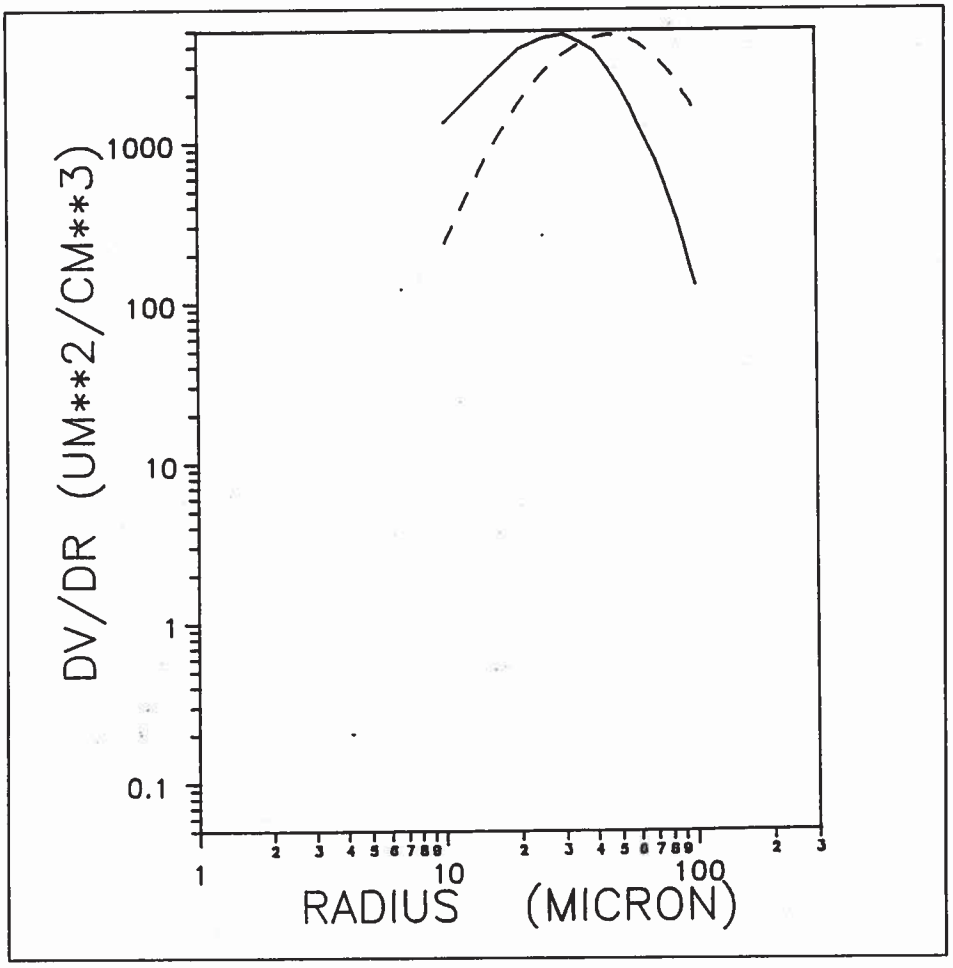

Figure 2a. Volumic concentration spectrum at a fixed height for the 19 drop categories ($\delta_{rn} = 5$ microns). $C_1 = 0.75, u_* = 0.49, z = 9.2$ cm.
—— : Model Cluse
- - - : Measurement (file 30 , 19 May, CLUSE-HEXIST3).

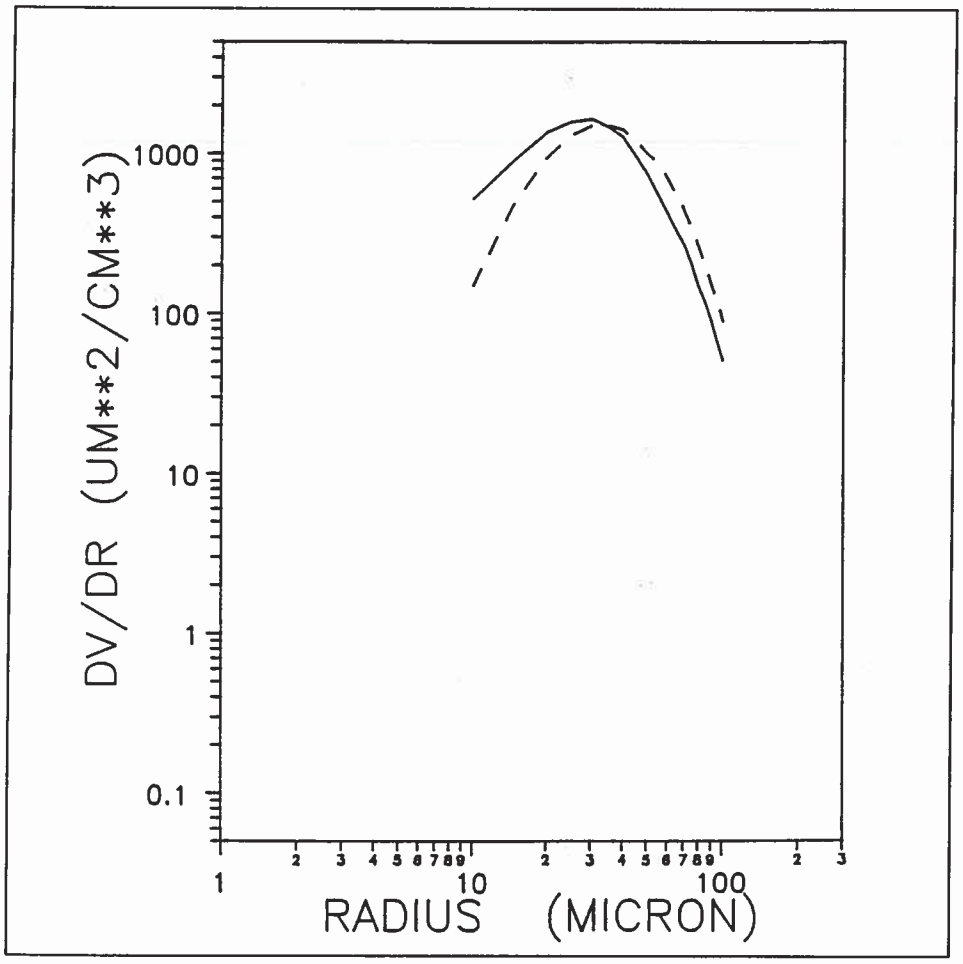

Figure 2b. Volumic concentration spectrum at a fixed height for the 19 drop categories ($\delta_{rn} = 5$ microns). $C_1 = 0.75, u_* = 0.49, z = 21.1$ cm.
—— : Model Cluse
- - - : Measurement (file 28 , 19 May, CLUSE-HEXIST3).

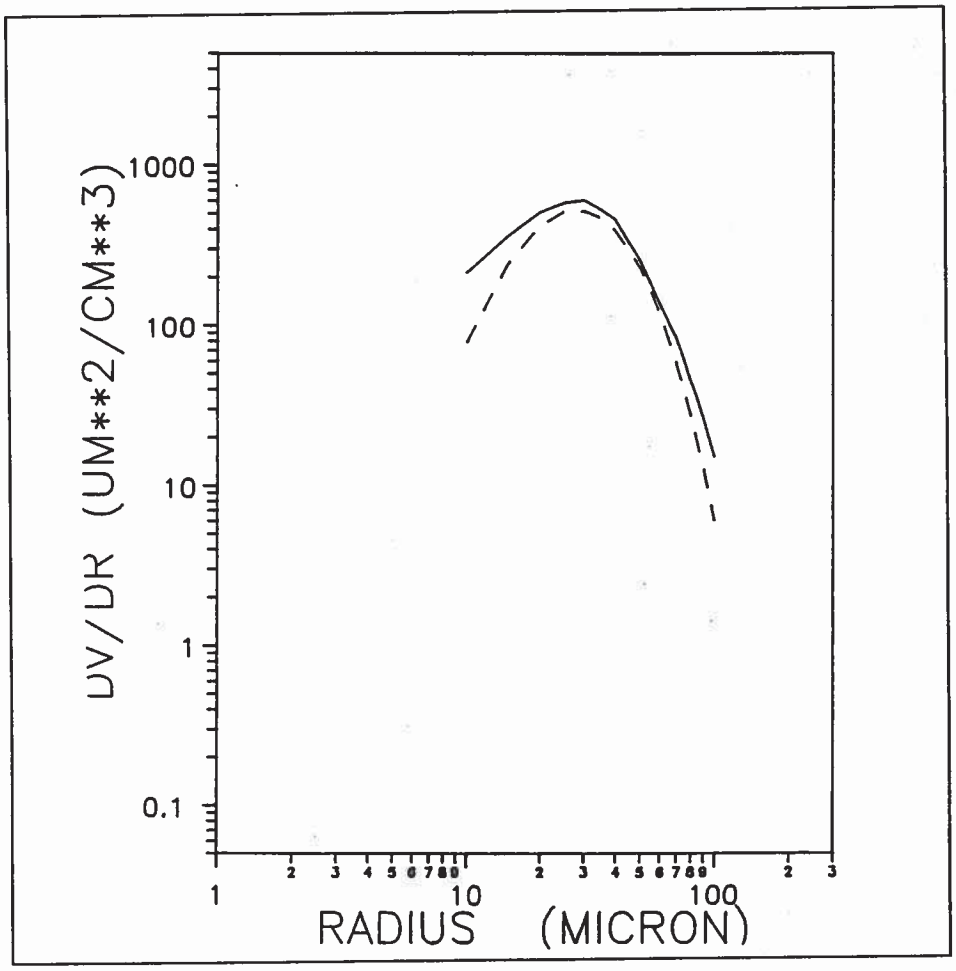

Figure 2c. Volumic concentration spectrum at a fixed height for the 19 drop categories ($\delta_{rn} = 5$ microns). $C_1 = 0.75, u_* = 0.49, z = 37.6$ cm.
—— : Model Cluse:
- - - : Measurement (file 26 , 19 May, CLUSE-HEXIST3).

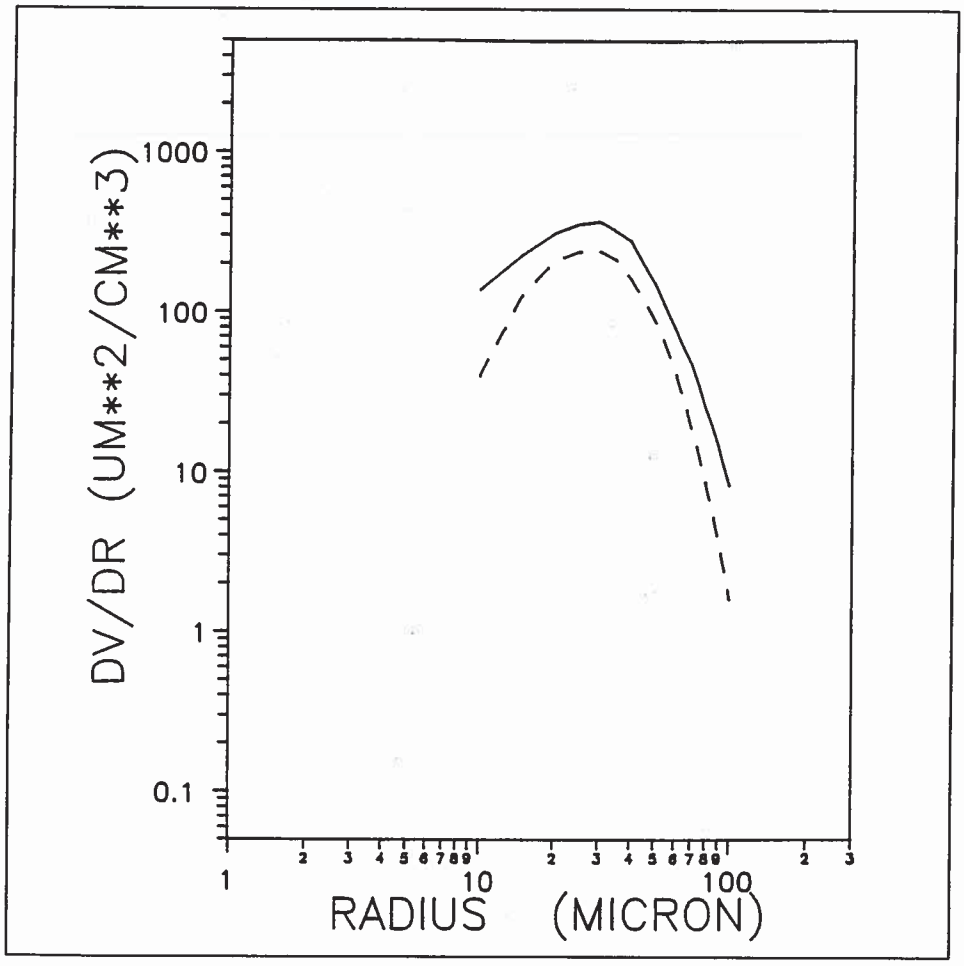

Figure 2d. Volumic concentration spectrum at a fixed height for the 19 drop categories ($\delta_{rn} = 5$ microns). $C_1 = 0.75, u_* = 0.49, z = 47.7$ cm.
—— : Model Cluse
- - - : Measurement (file 25 , 19 May, CLUSE-HEXIST3).

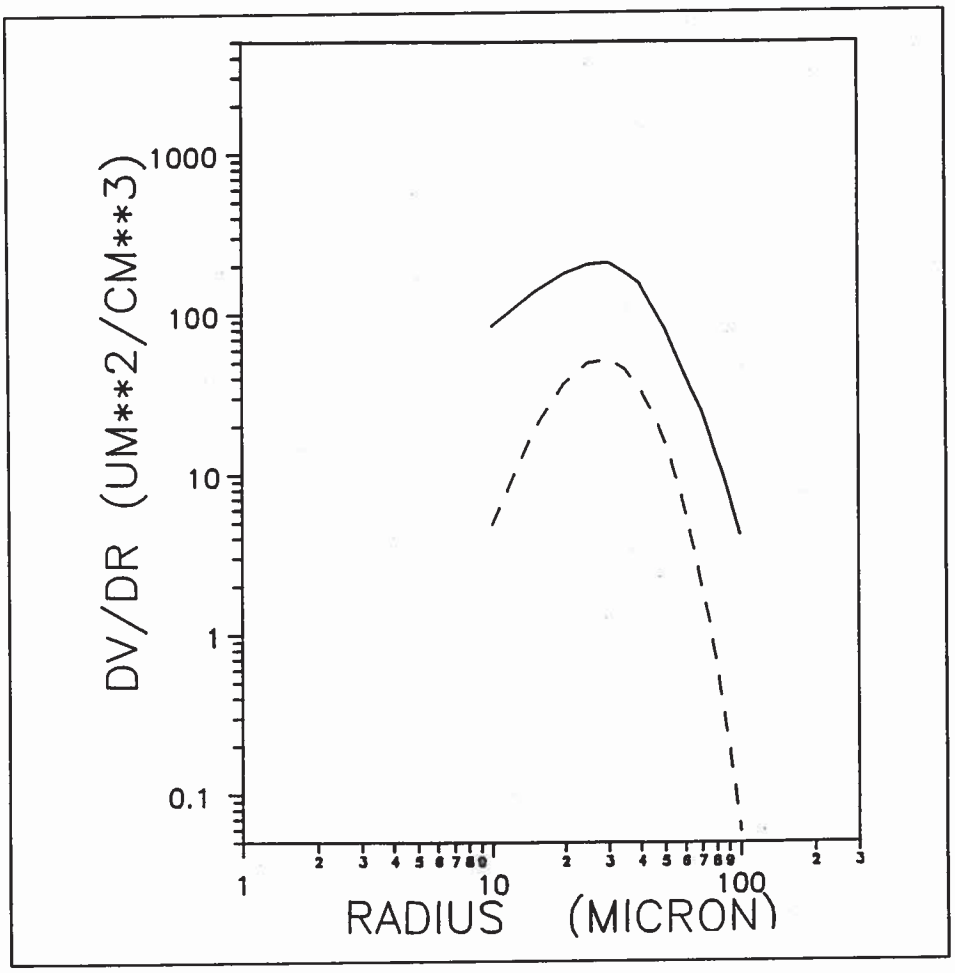

Figure 2e. Volumic concentration spectrum at a fixed height for the 19 drop categories ($\delta_{rn} = 5$ microns). $C_1 = 0.75, u_* = 0.49, z = 60.8$ cm.

—— : Model Cluse: ——

- - - : Measurement (file 23 , 19 May, CLUSE-HEXIST3).

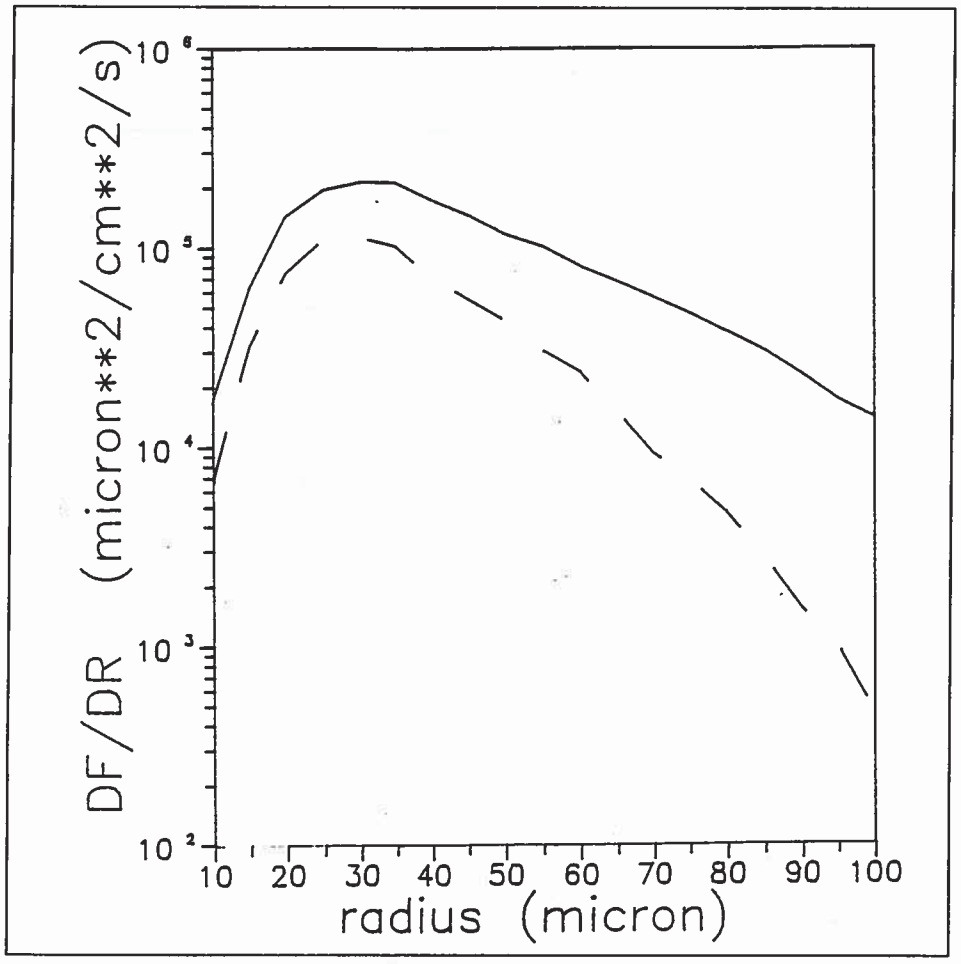

Figure 3. Ejected jet drop flux by radius incremeent (δ_{rn} = 5 microns) deduced from the 19 May measurements (files 22 to 30), the experiment made with all the bubblers: —— , compared with the ejected flux for the 23 May measurements (files 68 to 61), the experiment made with 1/3 of the bubblers: - - - - .

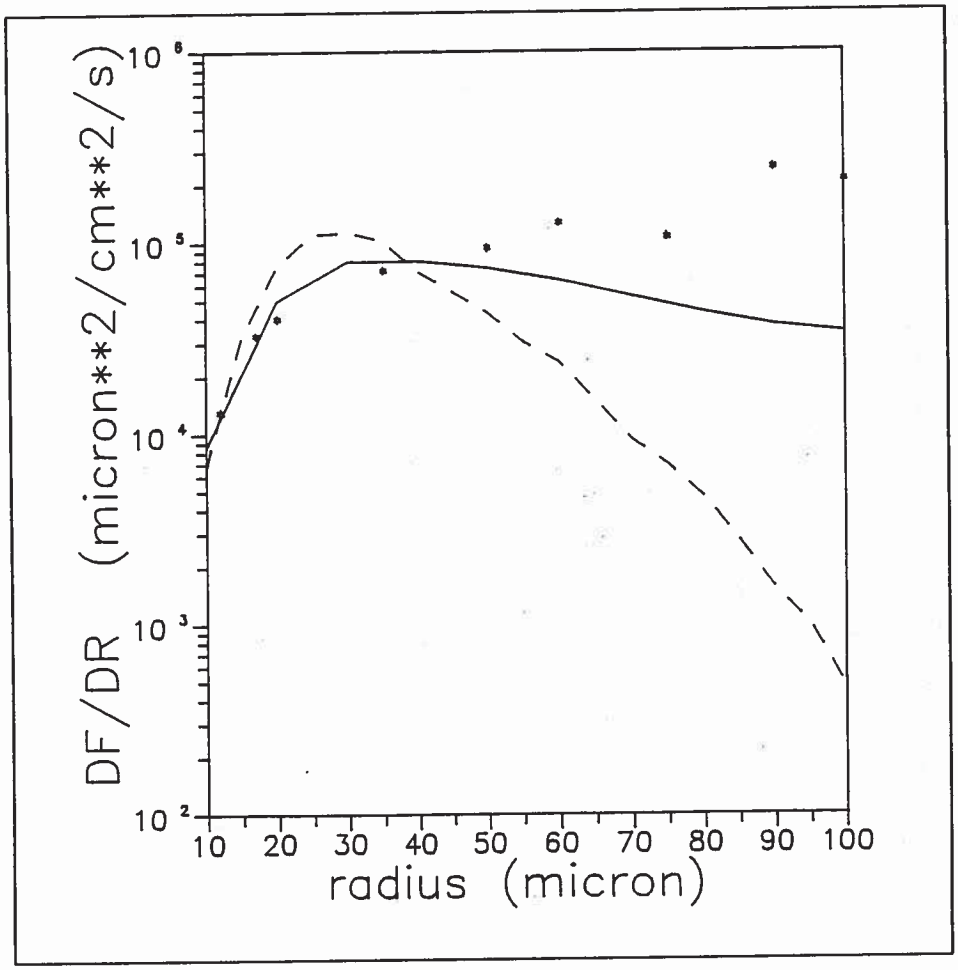

*Figure 4. Ejected jet drop flux (source function) by radius increment (δ_{rn} = 5 microns) deduced for the 23 May measurements (files 68 to 61), the experiment made with 1/3 of the bubblers: - - - compared to the modeled source function used by Edson (1989): —— and the source function adapted from the de Leeuw measurement by Edson: *.*

neglecting the counter diffusion term. The introduction of this term in the model allows an increase of the source function for the big droplets categories cf Figs. 6a and 6b). We have seen also an underestimation of the droplet distribution in our model experiment comparison for the big droplets close to the ejection height. This problem can be solved because even if we increase the source function for the big droplets, the counter diffusion term will reduce their distribution along the height of the domain and we could still have a good agreement with the experiment. On the same occasion we could solve the overestimation of the droplet distribution at the upper part (60 cm) because the counter diffusion term would decrease the distribution at this height. In the next paragraph we will show how this term is modeled and its effects on the vertical distribution of 10 to 100 microns droplets in turbulent conditions.

3.3 Modeling the counter diffusion

We assume that $\overline{\rho_n' w'}$, which appears in term 3 of Eq. (9), is related to the mean quantity gradients by an exchange coefficient K_n':

$$\overline{\rho'_n \Delta'_n} = -K'_n \frac{\partial \overline{\rho_n}}{\partial z} \tag{75}$$

We assume that K'_n reduces the turbulence diffusion. It will be proportional to K_n (Eq. (22)). It will also be proportional to the droplet radius. Taking into account Eqs. (16), (22) and (74) we can write Eq. (9)

$$\frac{\partial \overline{\rho_n}}{\partial t} = \frac{\partial}{\partial z}\left((K_n + K'_n)\frac{\partial \overline{\rho_n}}{\partial z}\right) - \frac{(\overline{\rho_n} - \rho_{on})}{C_1.T_{vn}} + S_n \tag{76}$$

Now we study the behaviour of the term $K_n + K'_n$ and we detail the ideas that produce the modeling of K'_n

a) The heavier the droplets, the greater is the reduction of the turbulence diffusion, so:

$$\text{When } r \to \infty \qquad K_n + K'_n \to 0 \tag{77}$$

b) The smaller the droplets, the more they behave like a gas (inertia negligible) and they have to follow the usual turbulence diffusion, thus:

$$\text{When } r \to 0 \qquad K_n + K'_n \to K_n \tag{78}$$

c) Then, for a given radius, the stronger the turbulence, the more the droplets behave like a gas. To characterize the turbulence, we choose the vertical velocity variance: $\overline{w^2} = 1.56\, U_*^2$

$$\text{When } u_* \to \infty \qquad K_n + K'_n \to K_n \tag{79}$$

To characterize the effect due to the radius variation,we use the final fall velocity V_f calculated in section A.3. All theses considerations lead to:

$$K_n + K'_n = K_n \left(1 + C_2 \frac{V_f^2}{1.56\, u_*^2}\right)^{-1} \tag{80}$$

where C_2 is a constant to be adjusted following a comparison with experimental data.

This result could be employed without considering a counter diffusion term. However, seeking a turbulence diffusion term that depends on droplet radius, one must look for an expression of the turbulent Schmidt number Sc_{t_n} (Section 2.1.4) function of the category n or the droplet radius. Figure 5 shows the variation of $(K_n + K'_n)/K_n$ as a function of the droplet radius when C_2 for three values of $u_*\{0.04, 0.27, 0.54\}$ which corresponds to $u_\infty = \{1$ m/s, 6 m/s, 12 m/s$\}$. The system of Eqs. (9), (10), and (11) is now closed and can be written:

$$\frac{\partial \overline{\rho_n}}{\partial t} = \frac{\partial}{\partial z}\left(\left(K_n \left(1 + C_2 \frac{V_f^2}{1.56\, u_*^2}\right)^{-1}\right)\frac{\partial \overline{\rho_n}}{\partial z}\right) - \frac{(\overline{\rho_n} - \rho_{on})}{C_1.T_{vn}} + S_n \tag{81}$$

$$\frac{\partial \overline{\rho_v}}{\partial t} = \frac{\partial}{\partial z}\left(K_v \frac{\partial \overline{\rho_v}}{\partial z}\right) - \sum_1^N S_n \tag{82}$$

$$\frac{\partial \overline{T}}{\partial t} = \frac{\partial}{\partial z}\left(K_t \frac{\partial \overline{T}}{\partial z}\right) + \frac{L_w}{\rho_a\, C_p} \sum_1^N S_n \tag{83}$$

In Fig. 6 we present the variation of the droplets volume spectra by radius increment in function of C_2 (C_2 = 10, 1, 0.1, 0.01), at a fixed height and for two wind speeds, u_∞ = 6 (Fig. 6a) and 12 m/s (Fig. 6b) (u_* = 0.27 and 0.54). We can see the results:

a) The turbulence diffusion by categories decreases when the radius increases

b The smallest droplets are apparently unaffected by the counter-diffusion

c) The stronger the turbulence, the less the droplets are affected.

C_2 must be adjusted by comparison measurement calculations when the data from CLUSE-HEXIST 3 will be available but we suppose that the effect of the counter diffusion is of second order and C_2 will be around 1.

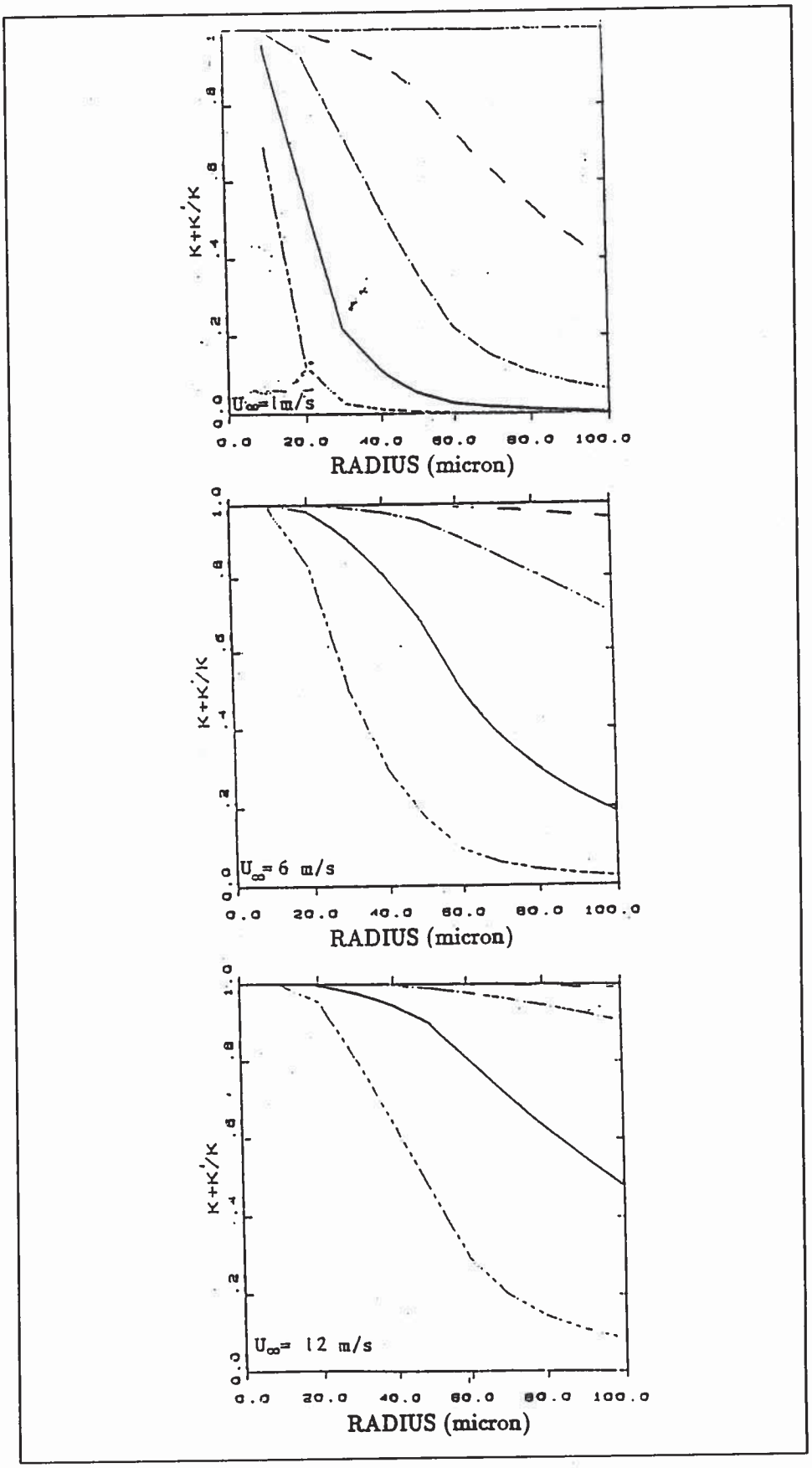

Figure 5. Relative reduction of turbulence diffusion in function of the droplet radius for three different reference wind speeds, $u_* = 0.54$ m/s (top), 0.27 m/s (mid), and 0.045 m/s (bottom). For each case $C_2 = 0.01$, 0.1, and 1.10.

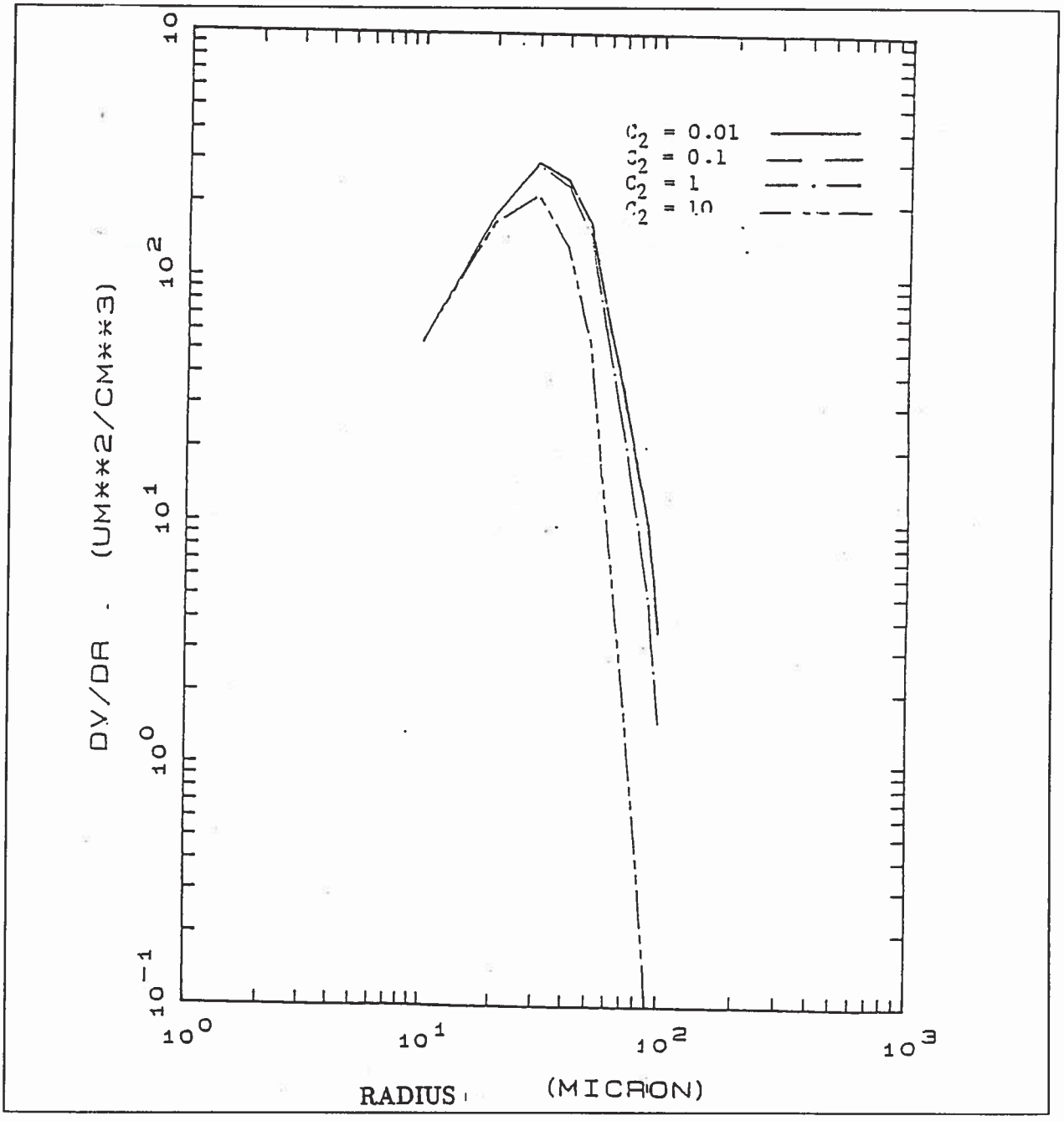

Figure 6a. Counter-diffusion influence on the volumic concentration spectra in function of different C_2-values. U_∞ = 12 m/s; u_* = 0.54 m/s; z = 40 cm.

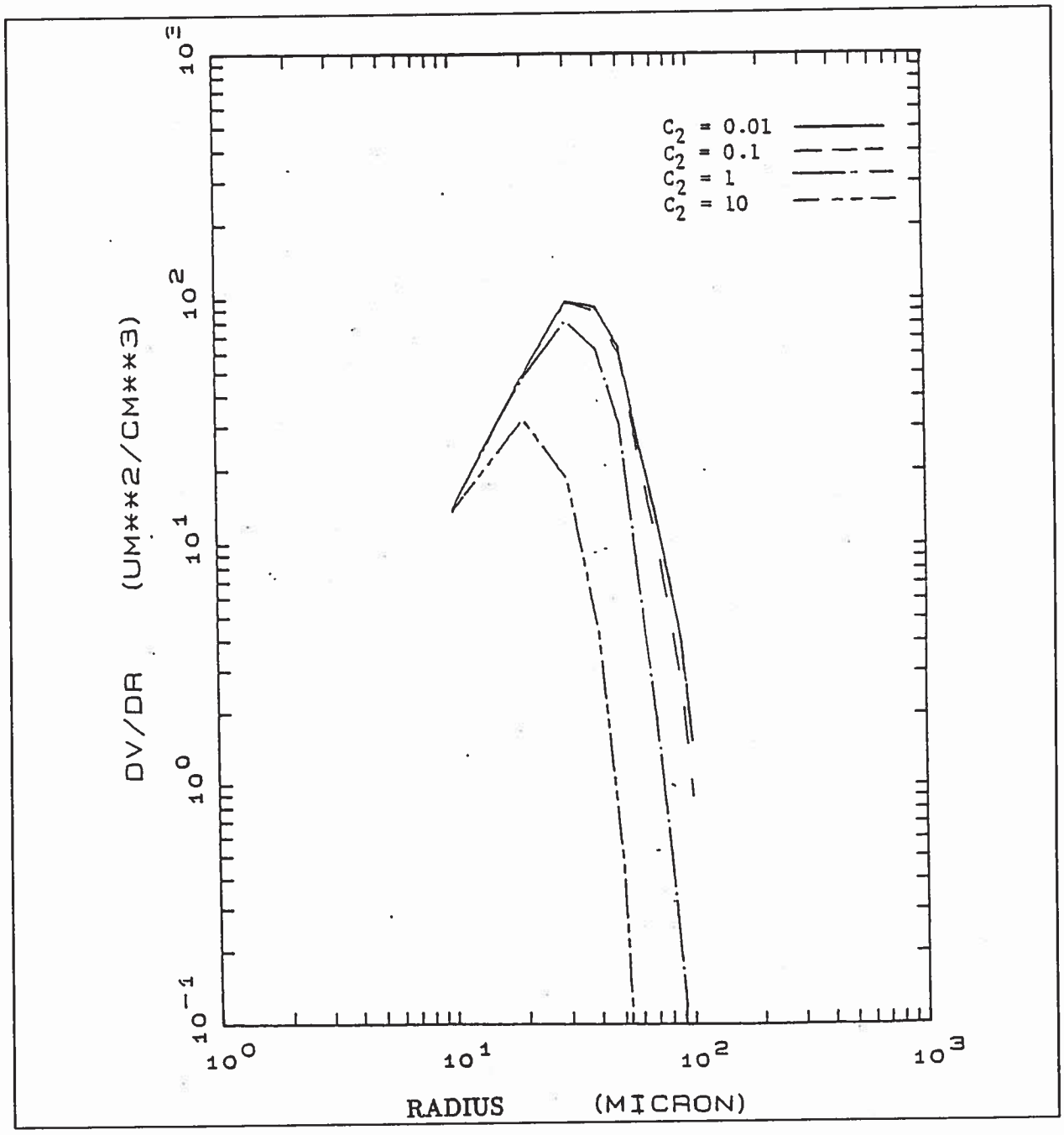

Figure 6b. Counter-diffusion influence on the volumic concentration spectra in function of different C_2-values. U_∞ = 6 m/s; u_* = 0.27 m/s; z = 40 cm.

4 The CLUSE model under evaporating and turbulent conditions

4.1 Calculation in evaporating conditions

To calculate ρ_{vsurf} we use the formulation (Buck, 1981):

$$\rho_{vsurf} = \rho_a \, (0.622 \, e_{vsurf}) \, / \, (P - 0.378 \, e_{vsurf}) \tag{84}$$

where

$$e_{vsurf} = 6.107 \, \exp \left(17.27 \, T_{surf} / \left(237.3 + T_{surf} \right) \right) \quad . \tag{85}$$

In the following calculation we introduce the relative humidity RH:

$$RH = 100 \, \rho_v \, / \, \rho_{vs} \tag{86}$$

where ρ_{vs} is calculated with Eq. (84). In the next section we use the ejected drop flux deduced from the 19 May. We have to define the boundary conditions, for the upper boundary ($z_{sup} = 2$ m):

$$\begin{aligned} T(z_{sup}) &= 26°\text{C} \\ RH(z_{sup}) &= 60\%. \end{aligned}$$

RH is related to the water vapor concentration ρ_v by the preceding relation or from the relations 59 and 60. Thus,

$$\rho_v(z_{sup}) = 0.0151 \ \text{kg/m}^3$$

for the droplets $\rho_n(z_{sup}) = 0$. For the lower boundary (at the water surface)

$$\begin{aligned} T(z_{sup}) &= T_{surf} = 20°\text{C} \\ RH &= 100\% \end{aligned}$$

Thus we can calculate ρ_v from Eq. (83):

$$\rho_v(z_{inf}) = 0.0174 \ \text{kg/m}^3.$$

We can now make a calculation for the 19 preceding droplet categories with $u_\infty = 9$ m/s. Thus, $u_* = 0.38$ m/s. The results are compared with the same case but without drop evaporation (Sn = 0). Figure 7 presents two droplet volumic spectra at two heights, $z = 60$ cm and $z = 20$ cm, respectively. We can see that the categories > 60 μm do not evaporate a lot because the evaporation function goes as $1/r$. In Figs. 8a, 8b, and 8c we present vertical profiles of volumic concentration per radius increment (δ_{r_n}=5 μm) for categories 10 μm, 50 μm, and 100 μm, and we have the confirmation of the preceding fact.

The results concerning the vertical temperature profile T and ρ_v are presented in Figs. 9 and 10. The profile in the non-evaporative case is characteristic of a flux constant layer and can be approximed by the equations:

$$T(z) = T_{surf} + T_* \frac{Pr_t}{\kappa} \log \left(z / z_{0c} \right) \tag{87}$$

$$\rho_v(z) = \rho_{v_{surf}} + \rho_{v_*} \frac{Sc_t}{\kappa} \log \left(z / z_{0v} \right) \tag{88}$$

where T_{surf} is the surface water temperature, $\rho_{v_{surf}}$ is the saturating water vapor concentration. z_0 is a roughness length; we use $z_0 = 1.5 \, 10^{-4}$ m and suppose that $z_0 = z_{0c} = z_{0v}$. With the constant flux hypothesis we can write in z_∞:

$$u_\infty = \frac{u_*}{\kappa} \log \left(z_\infty / z_0 \right) \tag{89}$$

Consequently, after Eqs. (85) and (86) we can deduce T_* and ρ_{v*}

$$T_* = \frac{\left(T_{v\infty} - T_{surf} \right)}{Pr_t \, U_\infty} \, u_* \tag{90}$$

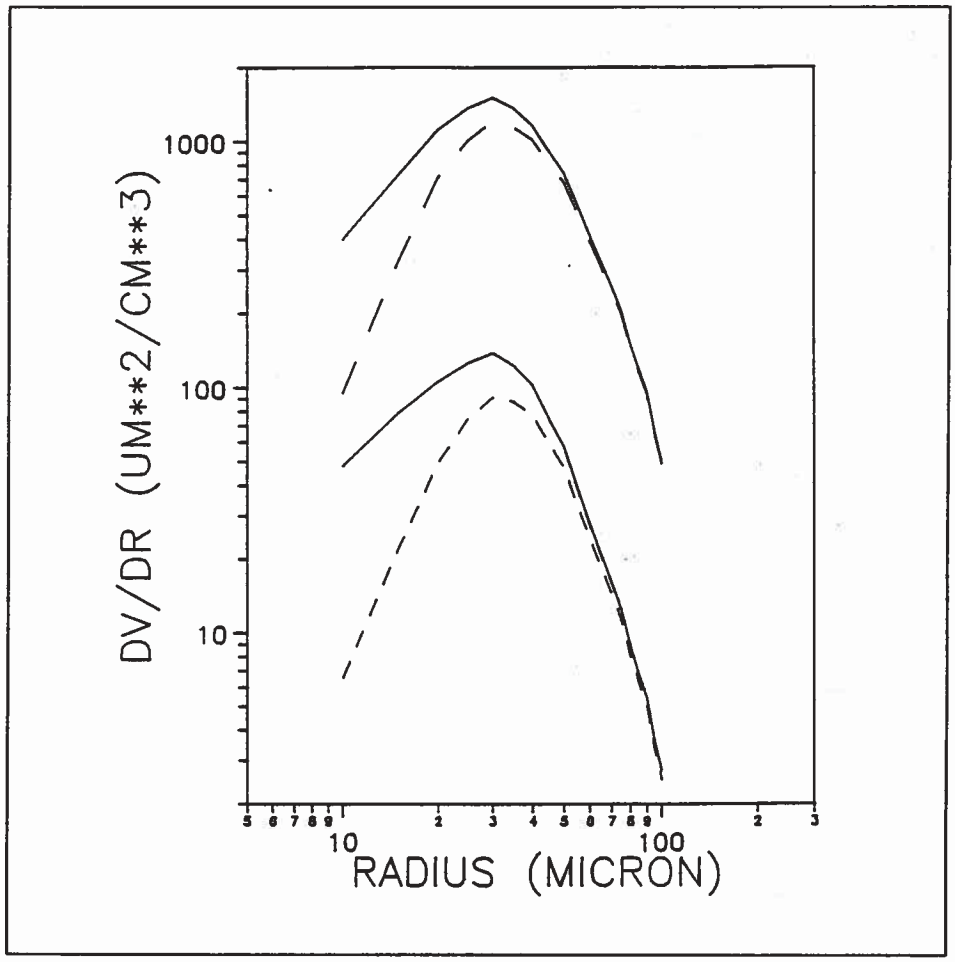

Figure 7. Volumic concentration spectra at two heights: 60 cm (bottom) and 20 cm (top), z_{sup} = 2m, $u_* = 0.38$ m/s, $\delta_{r_n} = 5\mu m$, non-evaporative case (–), T_{surf} = 20° C, $\rho_v(z_{inf}) = 0.0174$ kg/m^3, $T(z_{sup})$ = 26° C, evaporative case (- -).

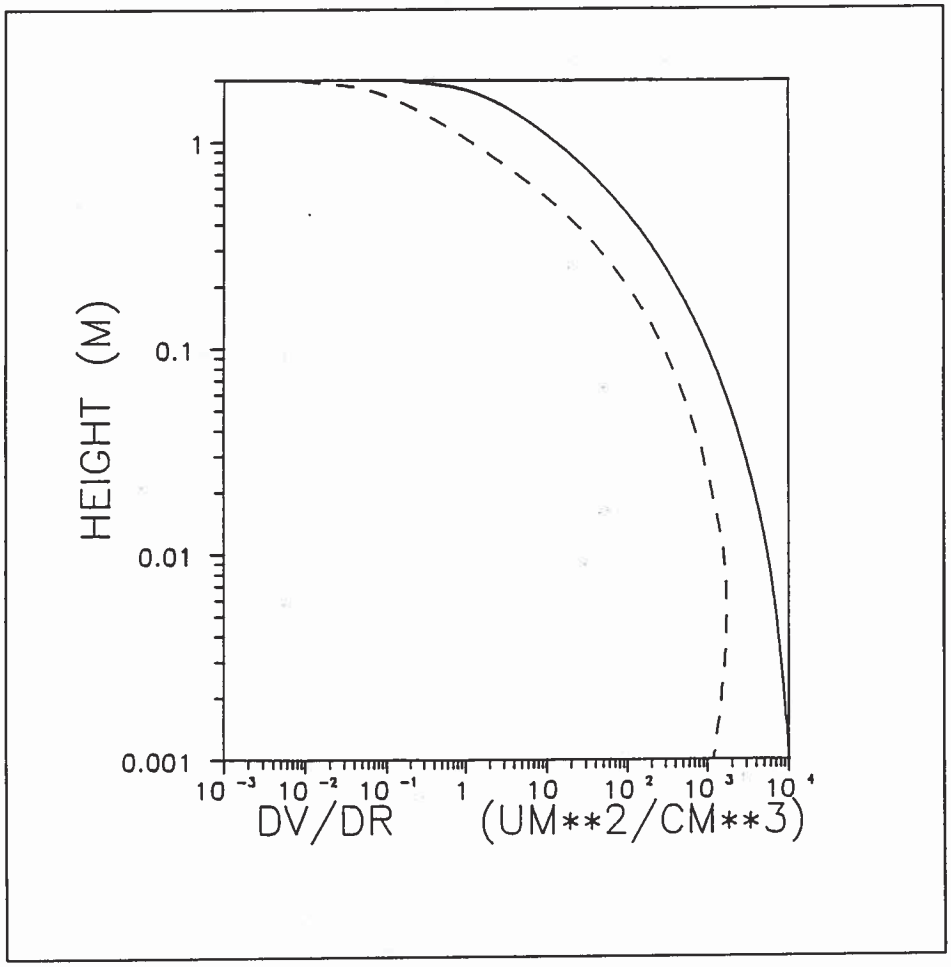

Figure 8a. Volumic concentration vertical profile of the 10 μm category, $z_{sup} = 2m$, $u_* = 0.38\ m/s$, $\delta_{r_n} = 5\mu m$, non-evaporative case: (–); $T_{surf} = 20°\,C$, $\rho_v(z_{inf}) = 0.0174\ kg/m^3$, $T(z_{sup}) = 26°\,C$, evaporative case: (- -).

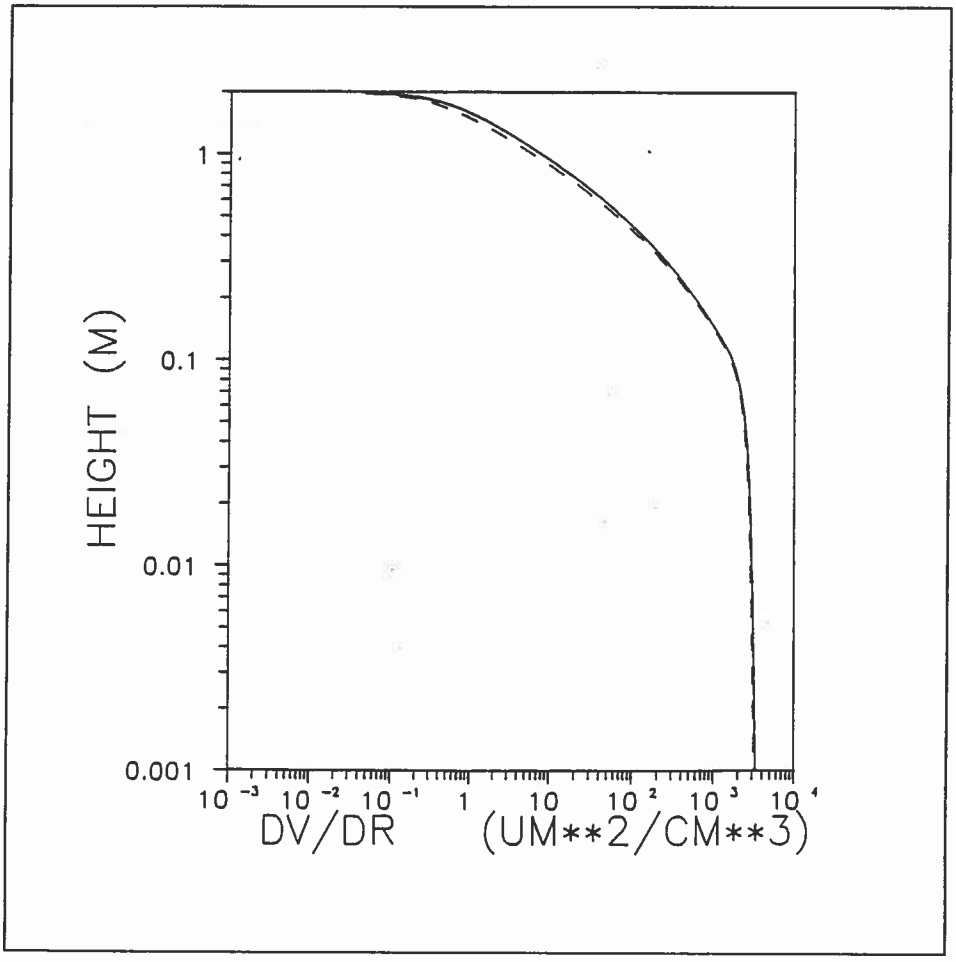

Figure 8b. Volumic concentration vertical profile of the 50 μm category, $z_{sup} = 2m$, $u_* = 0.38\ m/s$, $\delta_{r_n} = 5\mu m$, non-evaporative case: (-); $T_{surf} = 20°\,C$, $\rho_v(z_{inf}) = 0.0174\ kg/m^3, T(z_{sup}) = 26°\,C$, evaporative case: (- -).

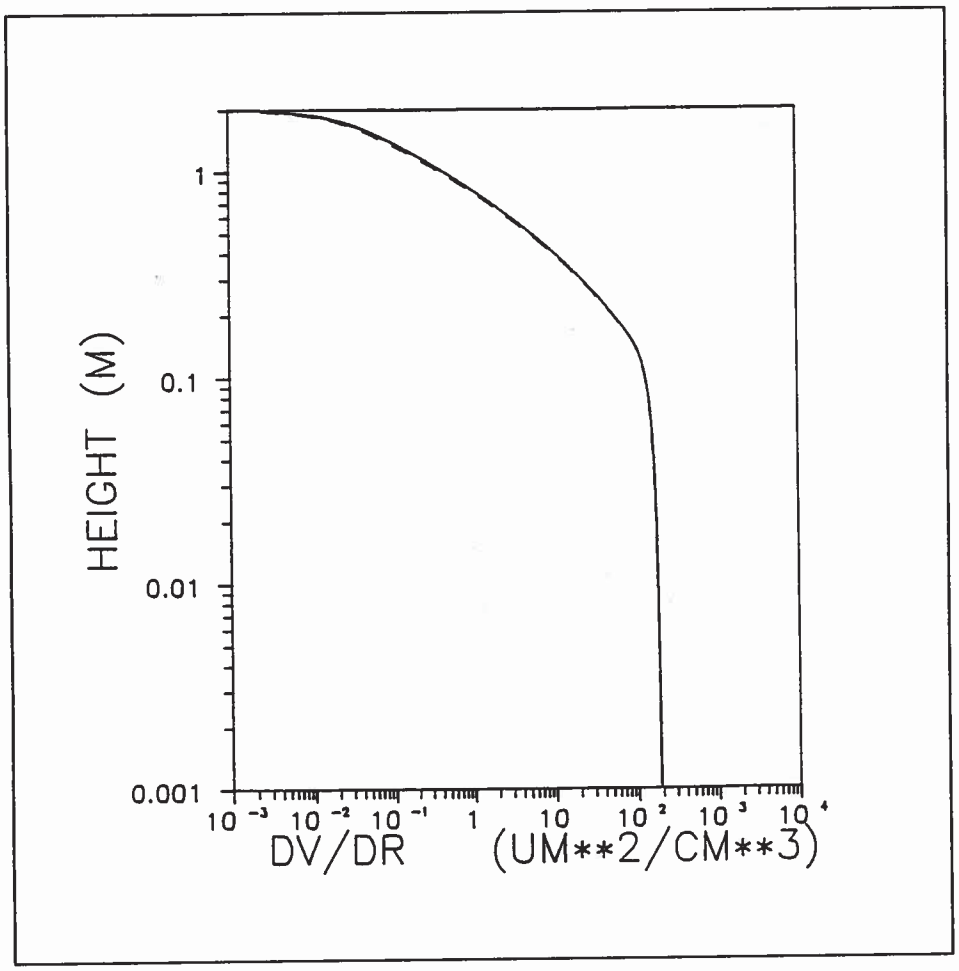

Figure 8c. Volumic concentration vertical profile of the 100 μm category, z_{sup} = 2m, $u_* = 0.38$ m/s, $\delta_{r_n} = 5\mu m$, non-evaporative case: (-); $T_{surf} = 20°C$, $\rho_v(z_{inf}) = 0.0174\ kg/m^3, T(z_{sup}) = 26°C$, evaporative case: (- -).

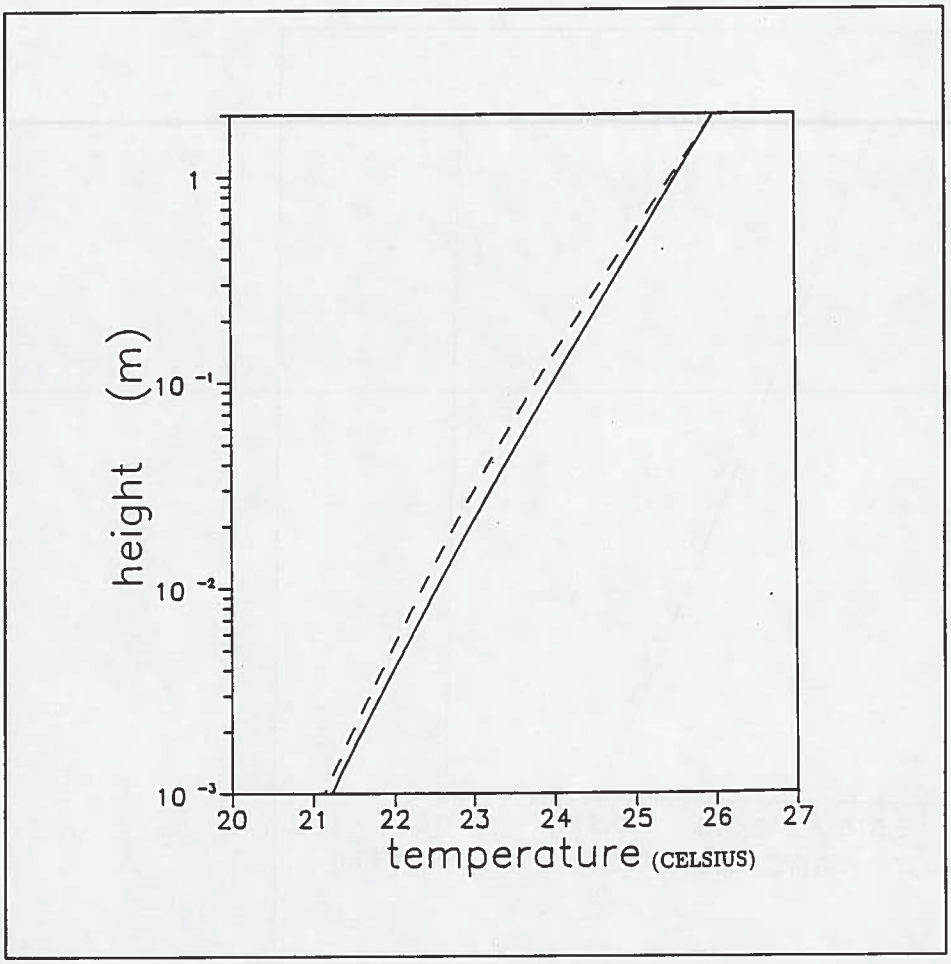

Figure 9. Vertical temperature profile, $z_{sup} = 2m$, $u_* = 0.38\ m/s$, $\delta_{r_n} = 5\mu m$, non-evaporative case: (–); $T_{surf} = 20°C$, $\rho_v(z_{inf}) = 0.0174\ kg/m^3$, $T(z_{sup}) = 26°C$, evaporative case: (- -).

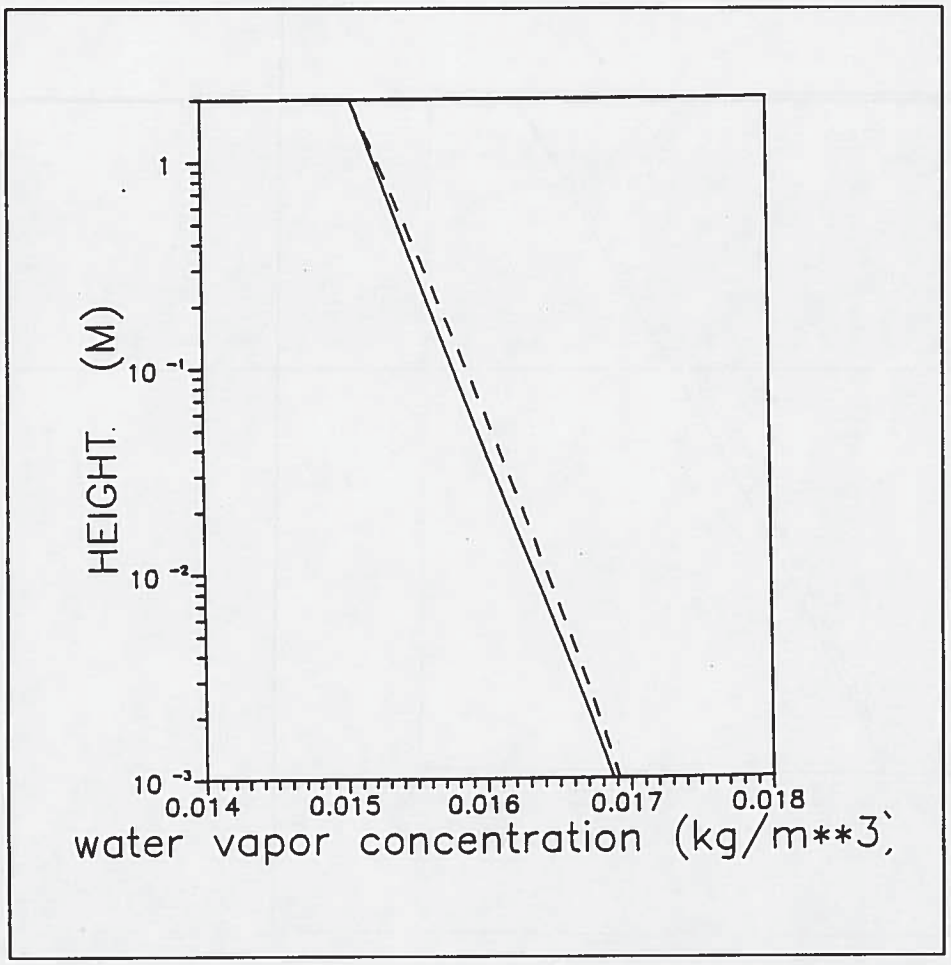

Figure 10. Vertical ρ_v-profile, $z_{sup} = 2m$, $u_* = 0.38\ m/s$, $\delta_{r_n} = 5\mu m$, non-evaporative case: (-); $T_{surf} = 20°C$, $\rho_v(z_{inf}) = 0.0174\ kg/m^3$, $T(z_{sup}) = 26°C$, evaporative case: (- -).

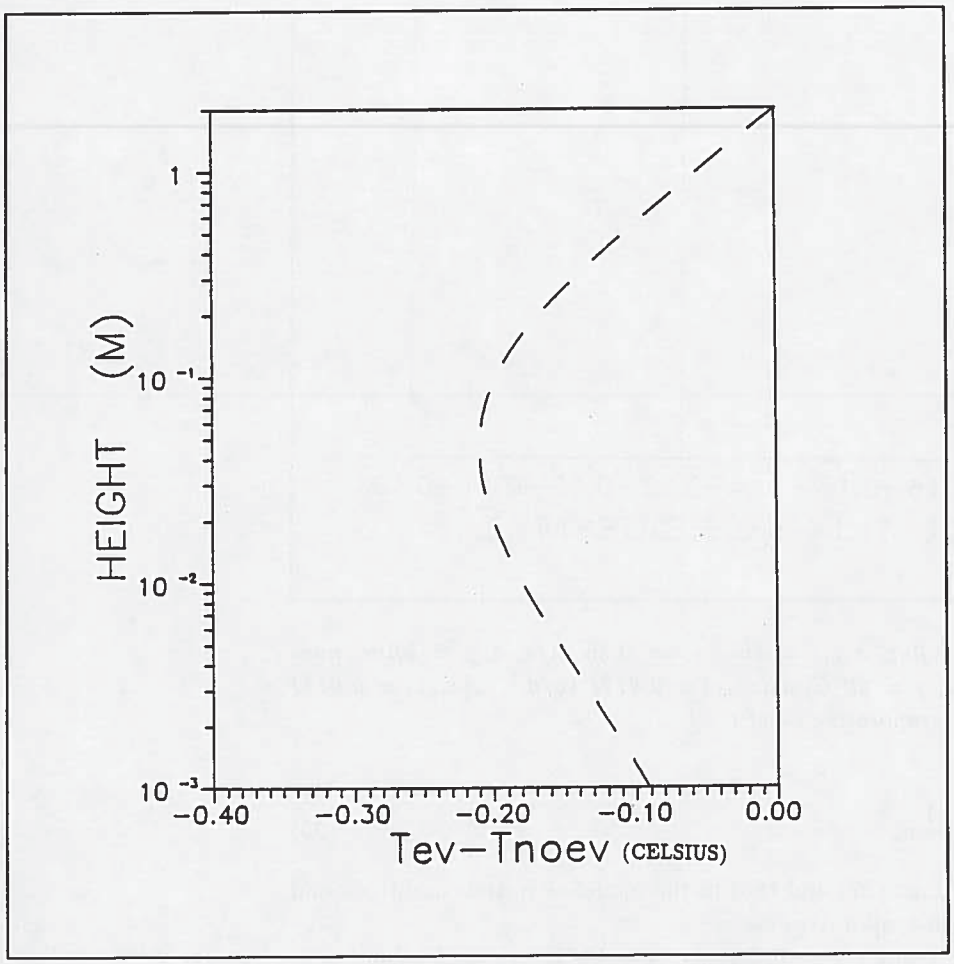

Figure 11. Temperature difference between evaporative and non-evaporative z_{sup} *=* $2m$*,* $u_* = 0.38\ m/s$*,* $\delta_{r_n} = 5\mu m$*, non-evaporative case: (-);* $T_{surf} = 20°C$*,* $\rho_v(z_{inf}) = 0.0174\ kg/m^3, T(z_{sup}) = 26°C$*, evaporative case: (- -).*

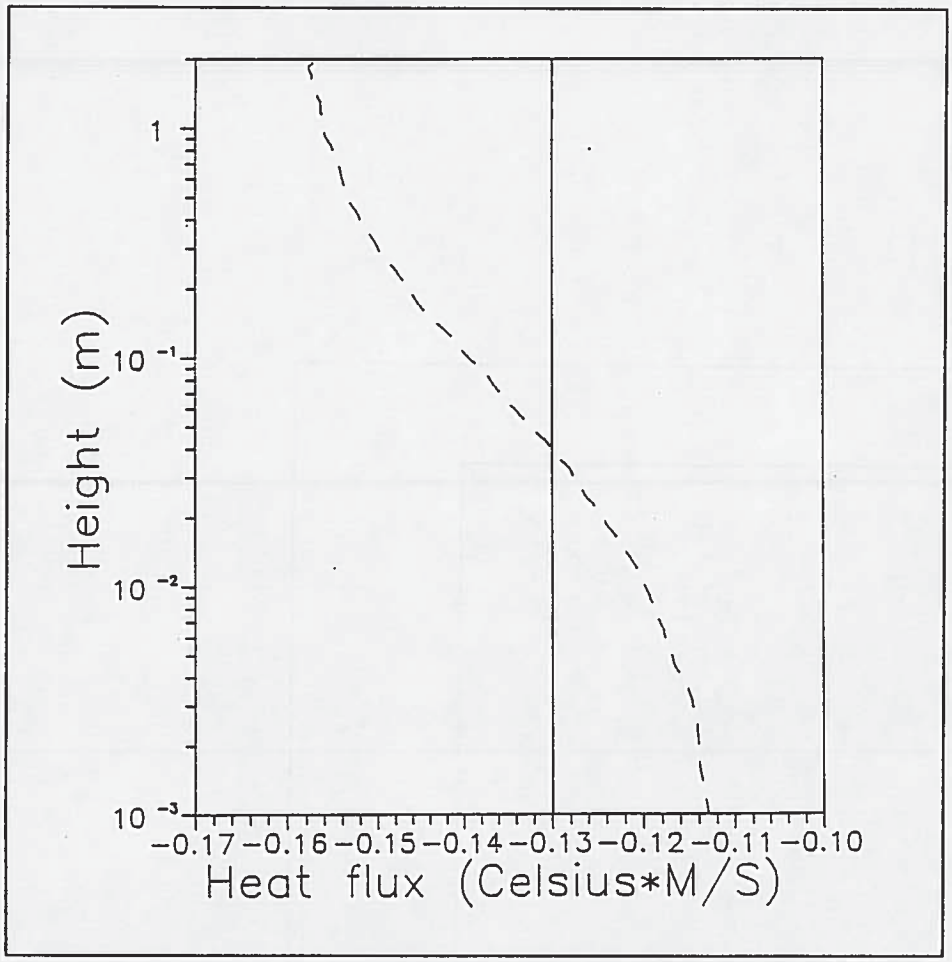

Figure 12. Vertical heat flux, $z_{sup} = 2m$, $u_* = 0.38\ m/s$, $\delta_{r_n} = 5\mu m$, non-evaporative case: (-); $T_{surf} = 20°C$, $\rho_v(z_{inf}) = 0.0174\ kg/m^3$, $\rho_v(z_{sup}) = 0.0151\ kg/m^3$, $T(z_{sup}) = 26°C$, evaporative case: (- -).

$$\rho_* = \frac{(\rho_{v\infty} - \rho_{vsurf})}{Sc_t\, u_\infty}\, u_* \tag{90}$$

with $z_\infty = z_{sup}$. We use Eqs. (87) and (88) in the model as initial conditions and to check the model in non-evaporative cases.

Figure 11 presents the temperature difference between an evaporative and non-evaporative case. We can see a maximum in the ejection area.

In Fig. 12 we also present the heat flux in an evaporative and non-evaporative case. The constant value for the non-evaporative case is characteristic of the flux constant layer and the in evaporative conditions cross the non-evaporative flux curve in the ejection area.

In conclusion we present the relative contribution of each S_n-term to S_v. We have $S_v = -\sum_1^N S_n$. In each control volume of our calculation domain we can calculate the ratio

$$A_n = S_n / \sum_1^N S_n \tag{91}$$

which represents the relative importance of each Sn to Sv at each height. However, in order to find the relative importance of each droplet category on the water vapor increase and temperature decrease due to their evaporation, it is better to integrate this relation throughout the domain:

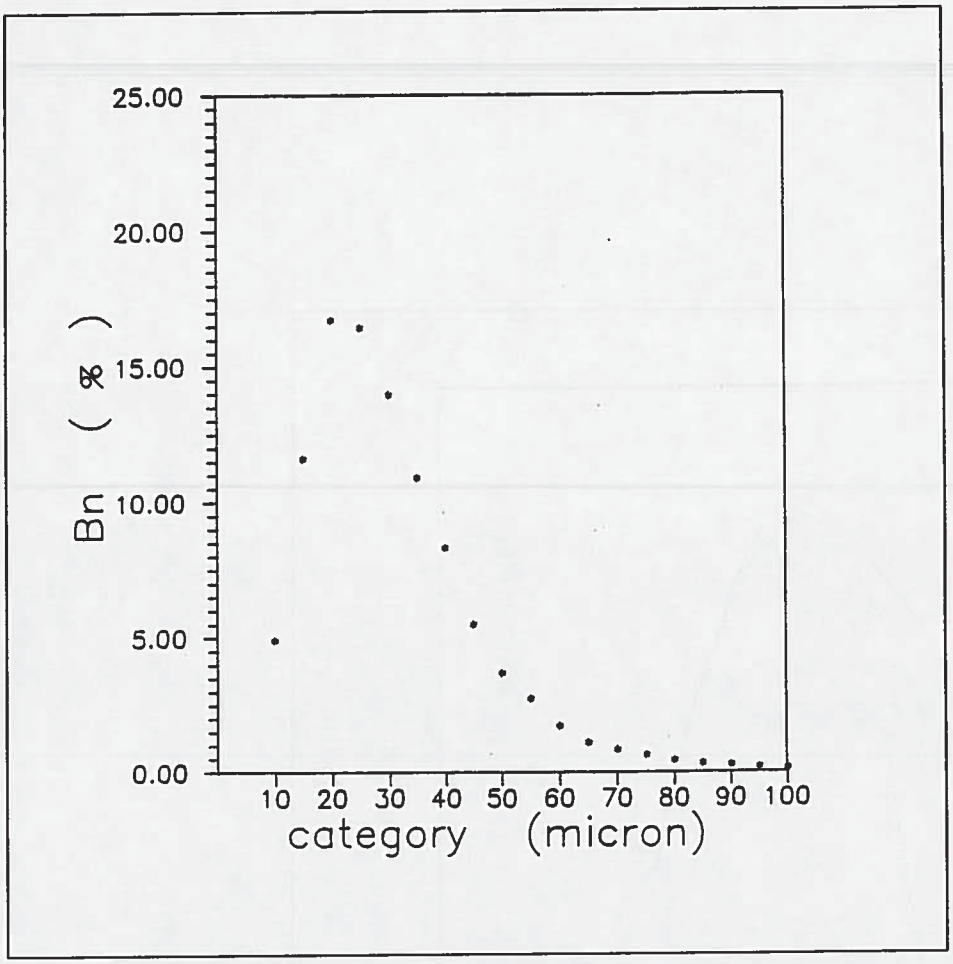

Figure 13. Relative contribution of each S_n-term to the humidity flux increase by evaporation. Category n corresponds to category 10 n μm. z_{sup} = 2 m, u_* 0 0.38 m/s, δ_{r_n} = 5 μm, non-evaporative case (-); T_{surf} = 20° C, $\rho_v(z_{inf})$ = 0.0174 kg/m^3, $\rho_v(z_{sup})$ = 0.0151 kg/m^3, $T(z_{sup})$ = 26° C, evaporative case: (- -).

$$B_n = \int_{z_{inf}}^{z_{sup}} S_n \, dz \; / \; \sum_{1}^{N} \int_{z_{inf}}^{z_{sup}} S_n \, dz \qquad (92)$$

The result is presented in Fig. 13. We can see that the 20 to 35 micron categories are the more important to the evaporation.

4.2 Calculation for different humidity configurations

We have made some calculations with different values of $\rho_v(z_{sup})$ corresponding to 80, 60, and 40% of relative humidity. We have kept the same values for z_{sup} $T(z_{sup})$, $T(z_{inf})$ and u_* in all three cases.

Now z_{sup} = 10 m high and we keep the same ejected drop flux than the preceding even if this flux is not wind related. This 10 meter cases is supposed to be a flux constant layer in natural conditions.

We see on Fig. 14 the variations of the droplet volumic spectra (z =3 0 cm) with the different humidity conditions compared with the same case without droplet evaporation (Sn = 0). In Fig. 15 we have the different temperature profiles. We can have a better understanding of the temperature profile modifications in Fig.

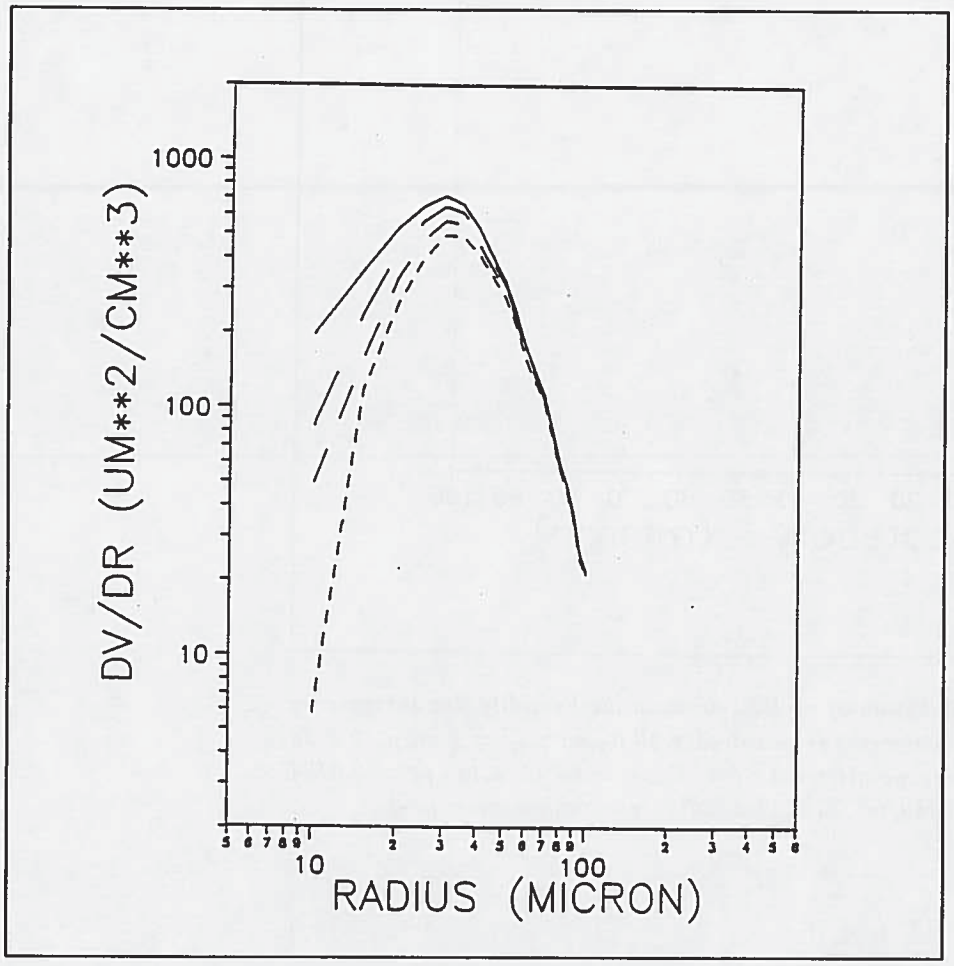

Figure 14. Volumic concentration spectra at 30 cm. $z_{sup} = 10$ *m,* $u_* = 0.36$ *m/s,* $\rho_{r_n} = 5\mu m$, *non-evaporative case:* ——— ; $T_{surf} = 20°C$, $\rho_v(z_{inf}) = 0.0150$ $kg/m^3, T(z_{sup}) = 26°C$; *evaporative case:*

— — — : $\rho_v(z_{sup}) = 0.0201, RH(z_{sup}) = 80\%$

- - - - - : $\rho_v(z_{sup}) = 0.0151, RH(z_{sup}) = 60\%$

- - - - - - : $\rho_v(z_{sup}) = 0.0100, RH(z_{sup}) = 40\%$.

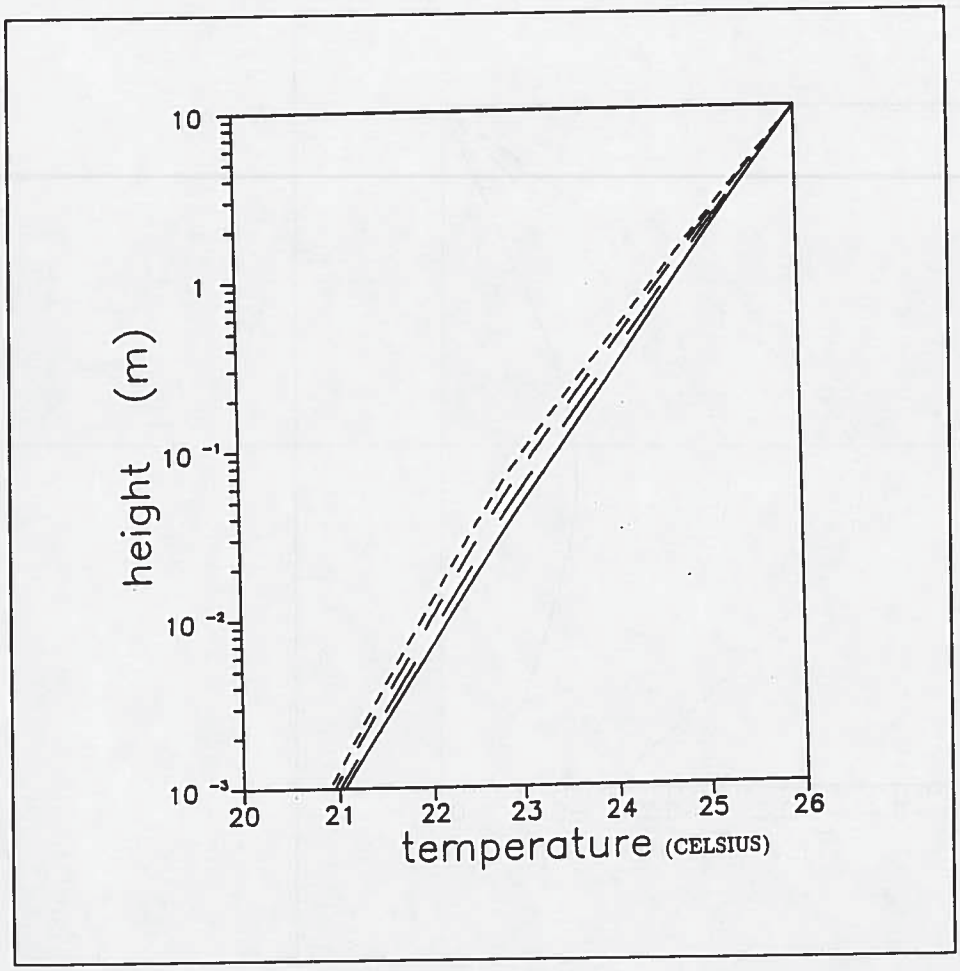

Figure 15. Vertical temperature profile. $z_{sup} = 10\ m$, $u_* = 0.36\ m/s$, $\rho_{r_n} = 5\mu m$, *non-evaporative case:* ——— ; $T_{surf} = 20°\,C$, $\rho_v(z_{inf}) = 0.0150\ kg/m^3, T(z_{sup})$ $= 26°\,C$; *evaporative case:*

— — — : $\rho_v(z_{sup}) = 0.0201, RH(z_{sup}) = 80\%$

– – – – – : $\rho_v(z_{sup}) = 0.0151, RH(z_{sup}) = 60\%$

- - - - - - : $\rho_v(z_{sup}) = 0.0100, RH(z_{sup}) = 40\%$.

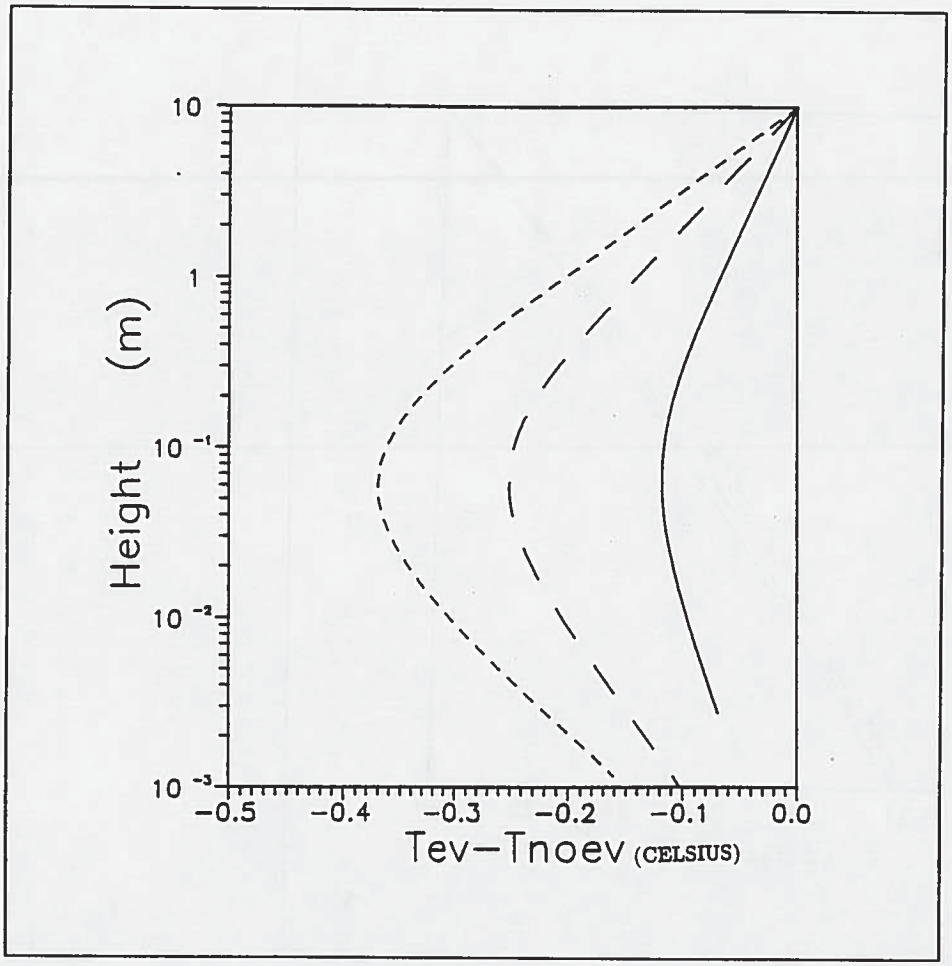

Figure 16. Temperature difference between the evaporative and non-evaporative case. $z_{sup} = 10$ *m,* $u_* = 0.36$ *m/s,* $\rho_{r_n} = 5\mu m$, *non-evaporative case:* ——— ; $T_{surf} = 20°C$, $\rho_v(z_{inf}) = 0.0150$ *kg/m*^{3}, $T(z_{sup}) = 26°C$; *evaporative case:*

— — — : $\rho_v(z_{sup}) = 0.0201, RH(z_{sup}) = 80\%$

- - - - - : $\rho_v(z_{sup}) = 0.0151, RH(z_{sup}) = 60\%$

- - - - - - : $\rho_v(z_{sup}) = 0.0100, RH(z_{sup}) = 40\%$.

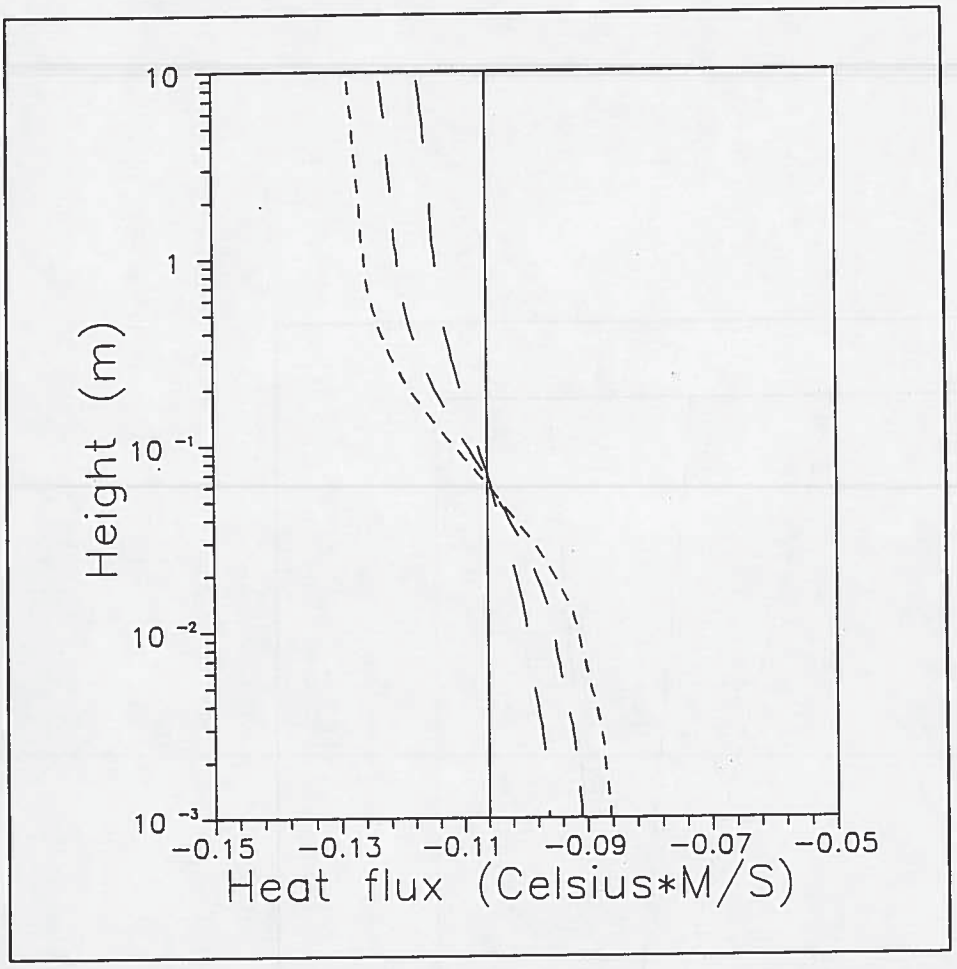

Figure 17. Vertical heat flux. $z_{sup} = 10$ *m,* $u_* = 0.36$ *m/s,* $\rho_{r_n} = 5\mu m$*, non-evaporative case: ——— ;* $T_{surf} = 20°C$*,* $\rho_v(z_{inf}) = 0.0150$ *kg/m*^{3}*,*$T(z_{sup}) = 26°C$*; evaporative case:*

— — —: $\rho_v(z_{sup}) = 0.0201, RH(z_{sup}) = 80\%$

– – – – –: $\rho_v(z_{sup}) = 0.0151, RH(z_{sup}) = 60\%$

– – – – – –: $\rho_v(z_{sup}) = 0.0100, RH(z_{sup}) = 40\%$.

16 where the difference between temperature in evaporating and non-evaporating cases are presented for each humidity cases. We see that the maximum is obtained for all cases in the area around the ejection zone. (1 to 30 cm).

We present in Fig. 17 an original result, the variation of the heat flux due to the droplet evaporation under different humidity conditions. If there is no droplet evaporation, this value is a constant. The less humid the layer, the more the heat flux is deformed around the constant value. The intersection point corresponds to the preceding maximum temperature difference height because the temperature difference increases from 0 to that height and then decreases to 0 again.

In Fig. 18 we present the water vapor concentration vertical profile for the three different humidity cases and in Fig. 19 the water vapor flux. The results is less spectacular but we can see the same shape for the flux than before (Fig. 17), especially for the 40% case.

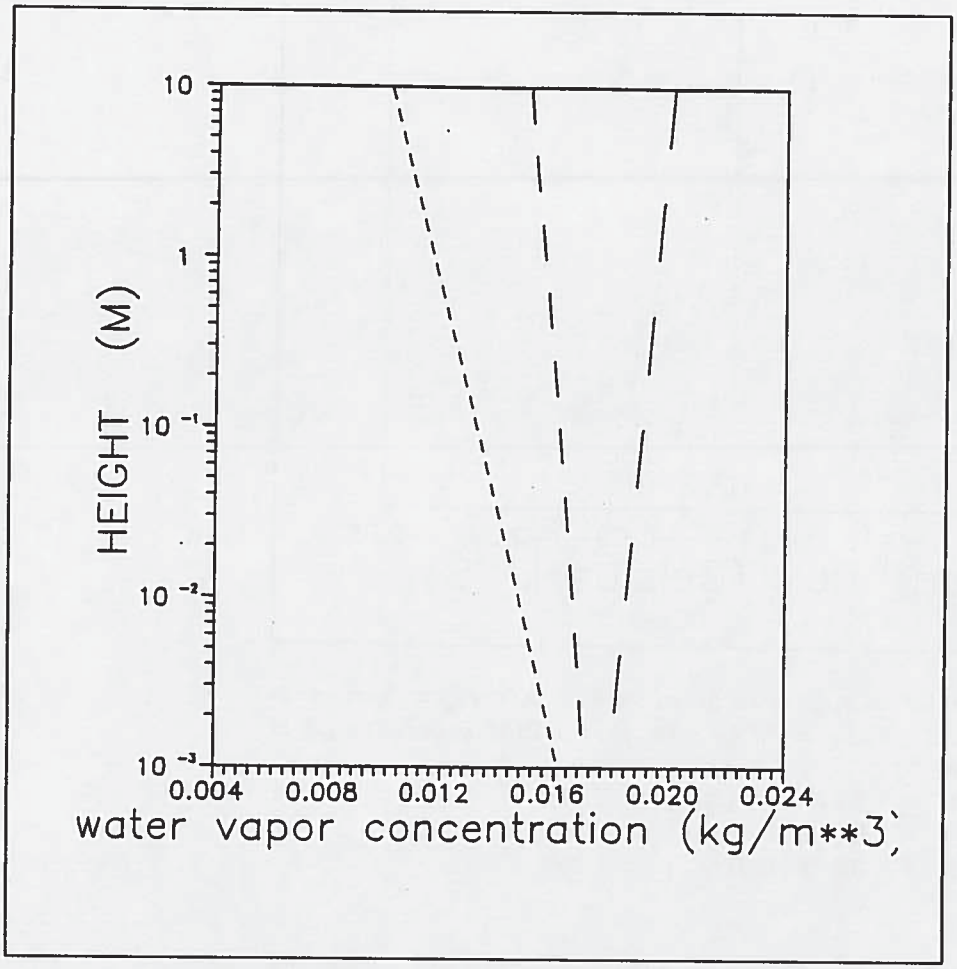

Figure 18. Vertical ρ_v- profile. z_{sup} = 10 m, $u_* = 0.36$ m/s, $\rho_{r_n} = 5\mu m$, non-evaporative case: ——— ; $T_{surf} = 20°C$, $\rho_v(z_{inf}) = 0.0150$ kg/m^3, $T(z_{sup}) = 26°C$; evaporative case:

— — — : $\rho_v(z_{sup}) = 0.0201, RH(z_{sup}) = 80\%$
- - - - - : $\rho_v(z_{sup}) = 0.0151, RH(z_{sup}) = 60\%$
- - - - - - : $\rho_v(z_{sup}) = 0.0100, RH(z_{sup}) = 40\%$.

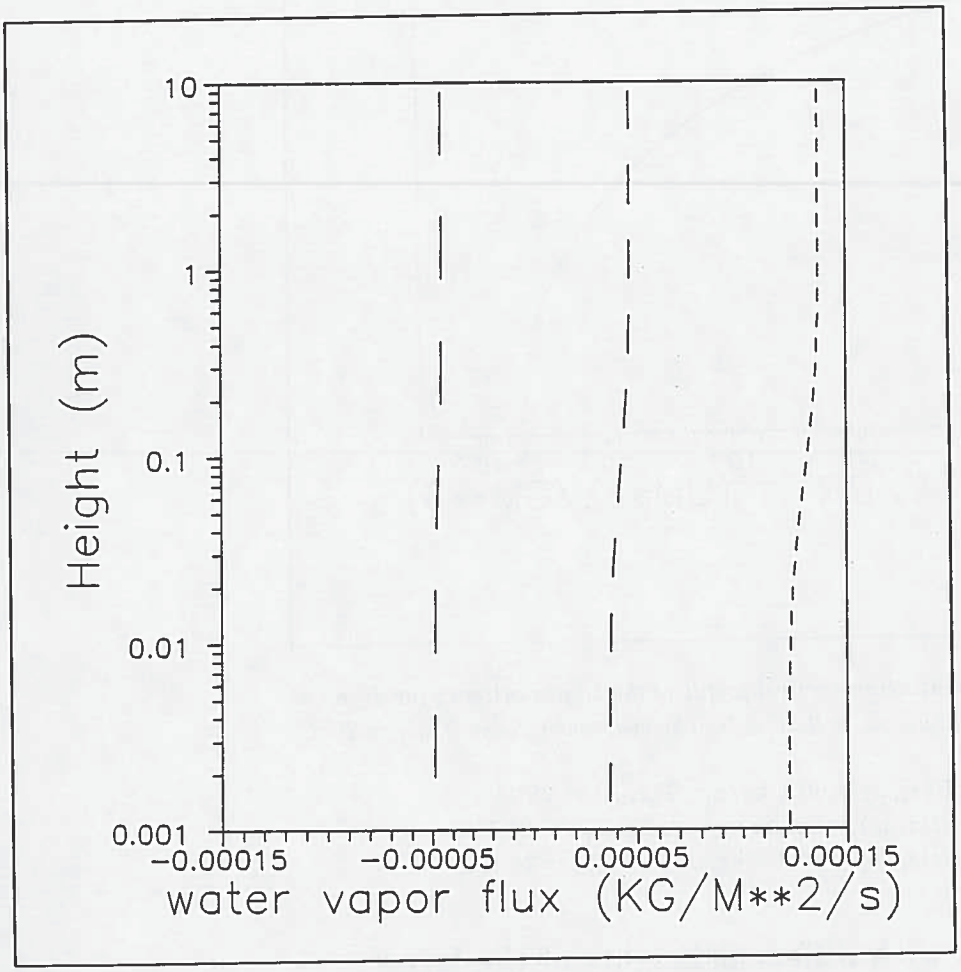

Figure 19. Vertical water vapor, ρ_v-flux. $z_{sup} = 10$ m, $u_* = 0.36$ m/s, $\rho_{r_n} = 5\mu m$, non-evaporative case: ——— ; $T_{surf} = 20°C$, $\rho_v(z_{inf}) = 0.0150$ kg/m^3, $T(z_{sup})$ = 26° C; evaporative case:

— — — : $\rho_v(z_{sup}) = 0.0201, RH(z_{sup}) = 80\%$

- - - - - : $\rho_v(z_{sup}) = 0.0151, RH(z_{sup}) = 60\%$

- - - - - - : $\rho_v(z_{sup}) = 0.0100, RH(z_{sup}) = 40\%$.

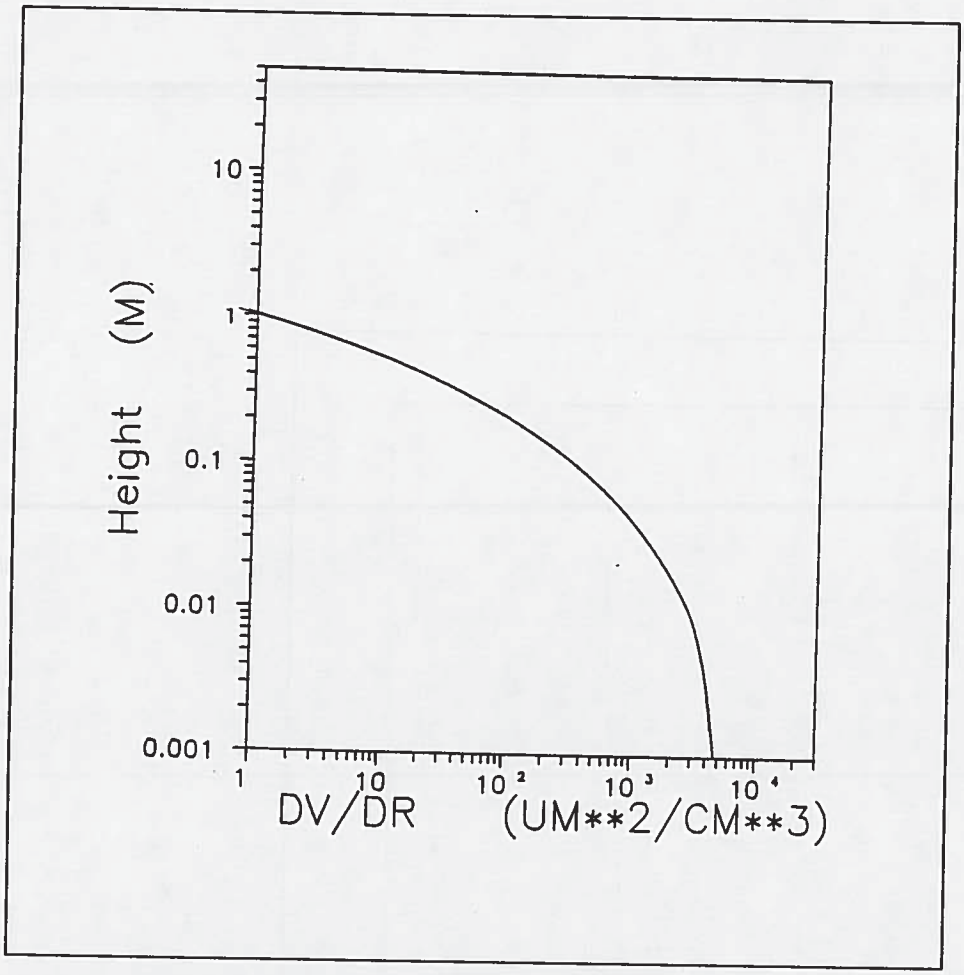

Figure 20. Volumic concentration vertical profile of the 50 μm category for different z_{sup} heights with constant u_*. $u_* = 0.36$ m/s. The evaporative case: $T_{surf} = 20°C$, $\rho_v(z_{inf}) = 0.0174$ kg/m^3
——— : $z_{sup} = 50$ m, $RH(z_{sup}) = 60\%$ kg/m^3, $T(z_{sup}) = 25°$C
- - - - : $z_{sup} = 25$ m, $RH(z_{sup}) = 61.7\%$ kg/m^3, $T(z_{sup}) = 24.7°$C
- - - - - : $z_{sup} = 10$ m, $RH(z_{sup}) = 64.1\%$ kg/m^3, $T(z_{sup}) = 24.4°$C.

4.3 Calculation with different heights of the layer

We have made some calculations with different values for z_{sup} ($z_{sup} = 10$, 25, and 50 meters). We have kept the same u_* in the three cases so we have the same values of turbulence diffusion in both cases. To do that we have employed the following upper boundary conditions:

$z_{sup} = 50$ m	$RH(z_{sup})$	=	60%	kg/m^3	$T(z_{sup}) = 25°$C
$z_{sup} = 25$ m	$RH(z_{sup})$	=	61.7%	kg/m^3	$T(z_{sup}) = 24.7°$C
$z_{sup} = 10$ m	$RH(z_{sup})$	=	64.1%	kg/m^3	$T(z_{sup}) = 24.4°$C

We present in Fig. 20 the volumic concentration vertical profile of the 10 μm category. There is no apparent change between the three cases, they are on the same curve. Only below 8 m there are some changes but as can be seen in Fig. 20, the concerned values are too small to influence the evaporation. The temperature and humidity profile are also the same.

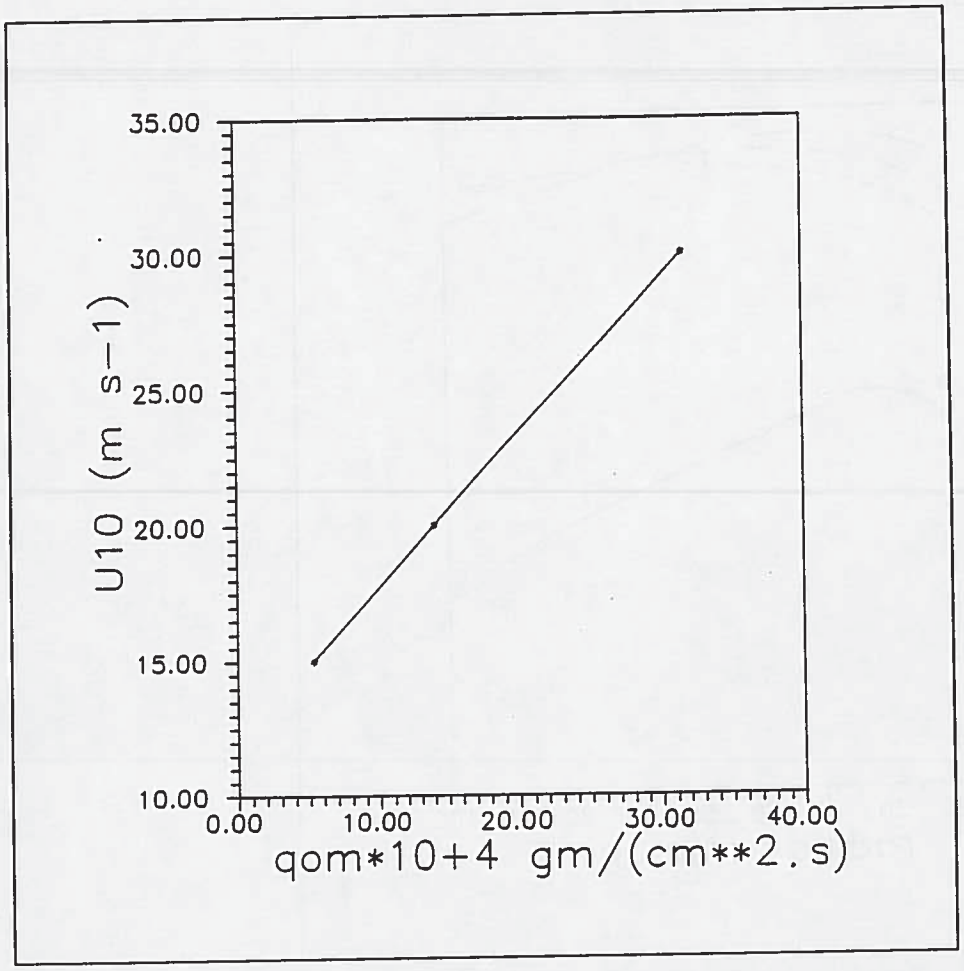

Figure 21. Vertical mass flux in spray, generated at the interface after Bortkovski in function of the wind speed at 10 meters.

In conclusion we can say that whatever the conditions are, the most productive area in water vapor (by drop evaporation) even in turbulent conditions, is around the ejection zone from 1 to 30 cm. It is a short area close to the surface and this makes the measurements difficult in natural condition with waves.

4.4 Ejected drop flux after Bortkovskii

Bortkovskii (1986) uses a distribution function for the drop sizes:

$$F(r) = 4\frac{r^2}{r_m^3}\exp\left(-2\frac{r}{r_m}\right) \tag{94}$$

where r_m is the mode radius of the spray drops with 0.003 cm $< r_m <$ 0.006 cm. The vertical mass flux in spray is given for all drops. It is a function of whitecap coverage, S_{wc}, and the wind speed at 10 meters:

$$q_{0_m} = 3.5\ 10^{-5}\ u_{10}\ S_{wc} \tag{95}$$

For u_{10} = 15, 20, 30 m/s, the vertical mass flux in spray is 5.25 10^{-4}, 14 10^{-4}, 31.5 10^{-4} gm (cm^2 s)$^{-1}$ (see Fig. 21)

In our study we need the vertical drop flux by categories if we use the distribution function F we have:

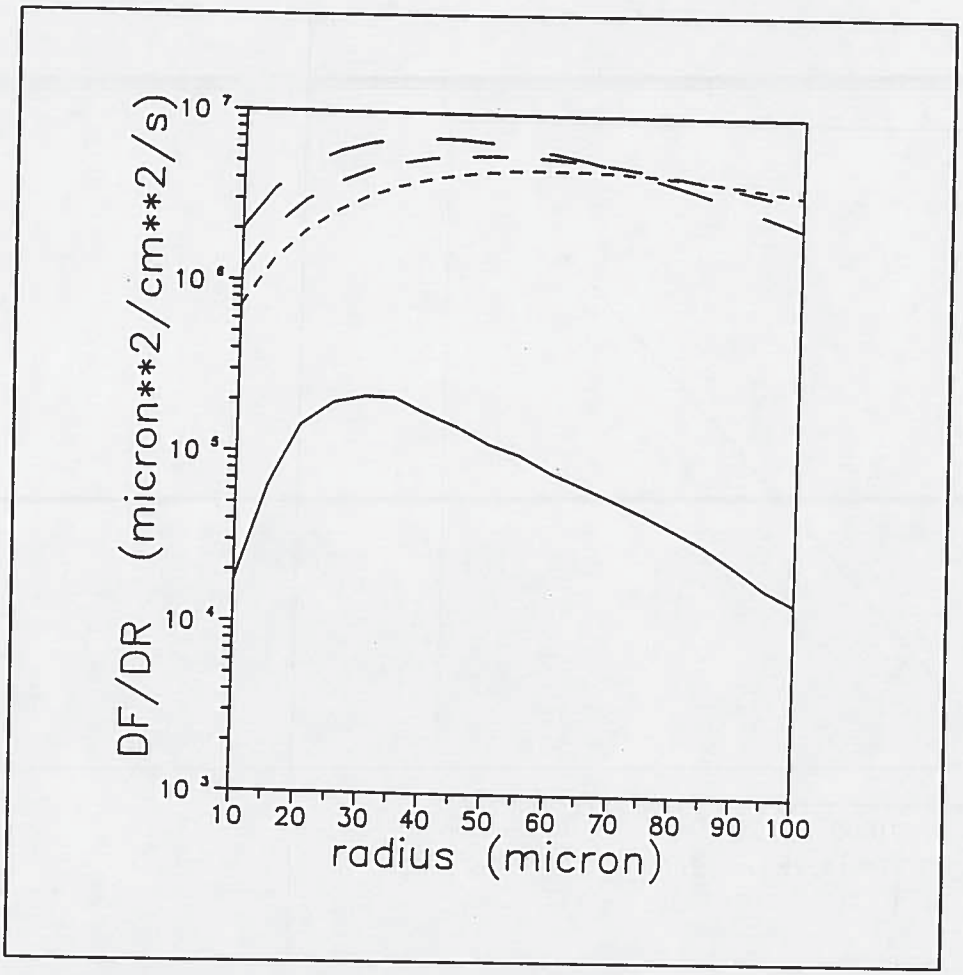

Figure 22. Ejected jet drop flux by radius increment, (δ_m = 5 microns) for each drop category deduced for the 19 May measurements (files 22 - 30), experiment made with all the bubblers: ——— , compared with the ejected flux after Bortkovski for different values of the model radius.
— — — : r_m = 40 microns
- - - - - : r_m = 50 microns
- - - - - - : r_m = 60 microns.

$$q_{0_m}(r_n - \delta_{r_n}/2 < r_n < r_n + \delta_{rn}/2) = q_{0_m} \int_{r_n+\delta_{rn}/2}^{r_n+\delta_{rn}/2} F(r)dr \qquad (96)$$

$$= -\frac{q_{0_m}}{r_m^2}\left((2\,r_1^2 + 2r_m r_1 + r_m^2)\ \exp\left(-2\frac{r_1}{r_m}\right)\right.$$

$$\left. - (2r_2^2 + 2r_m r_2 + r_m^2)\exp\left(-2\frac{r_2}{r_m}\right)\right) \qquad (97)$$

We use three r_m-values. In Fig. 22 we present the three corresponding fluxes by category for the 19 categories ($r_n = 10, 15, 20, \ldots 100$ micrometers and $\delta_{rn} = 5$ micrometers). Theses flux are a lot more important than the flux deduced from the comparisons between the model CLUSE and the CLUSE-HEXIST3 experiment. But from 9 m/s to 15 m/s it is obvious that the spray flux increases a lot.

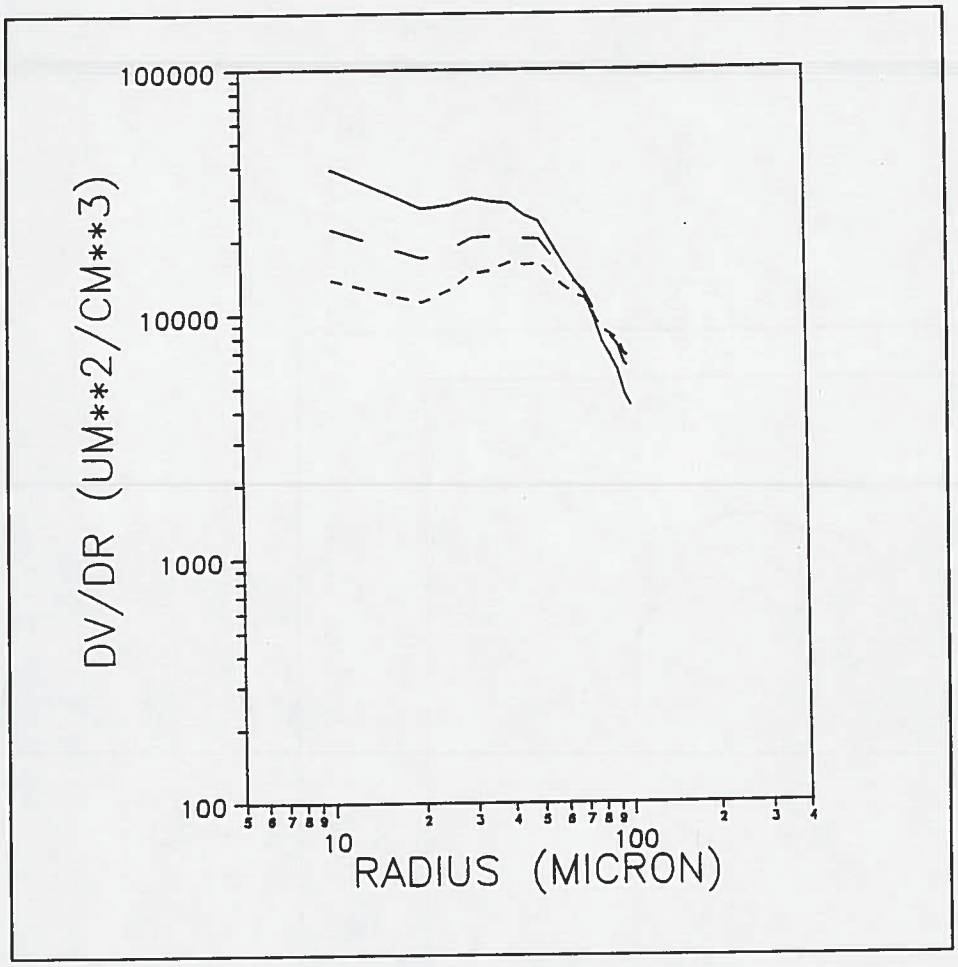

Figure 23. Volumic concentration spectra at 30 cm, $z_{sup} = 10$ m, $u_* = 0.54$ m/s, $\delta_{r_n} = 5\mu m$, the non-evaporative case.
———— : $r_m = 40$ microns
— — — : $r_m = 50$ microns
- - - - - : $r_m = 60$ microns.

We use these fluxes in a calculation under the usual conditions for a 15 m/s u_{10} wind velocity, so $u_* = 0.54$.

z_{sup}	=	10 m
$T(z_{sup})$	=	25°C
$\rho_v(z_{sup})$	=	0.0142 kg/m^3
T_{surf}	=	20°C
$\rho_v(z_{inf})$	=	0.0174 kg/m^3

We present the usual result compared to the equivalent case without drop evaporation. In Fig. 23 we present the drop spectra by radius increment at 30 cm with no drop evaporation and in Fig. 24 with drop evaporation; the temperature vertical profile (Fig. 25); the water vapor concentration profile (Fig 26), and their respective flux (Figs. 27 and 28).

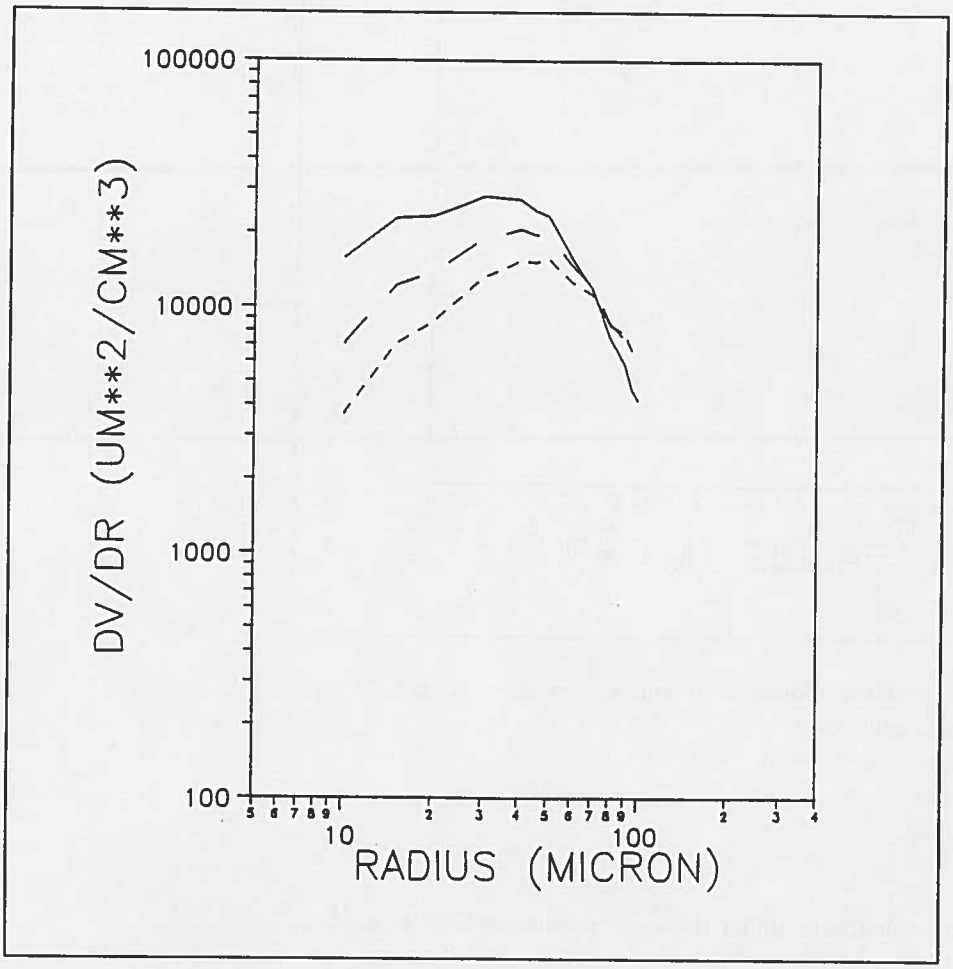

Figure 24. Volumic concentration spectra at 30 cm, $z_{sup} = 10$ m, $u_* = 0.54$ m/s, $\delta_{r_m} = 5\mu m$, the evaporative case. $T_{surf} = 20°C$, $\rho_v(z_{inf}) = 0.0174$ kg $m^3, \rho_v(z_{sup}) = 0.0142$ kg/$m^3, T(z_{sup}) = 25° C$.

——— : $r_m = 40$ microns

— — — : $r_m = 50$ microns

- - - - - : $r_m = 60$ microns.

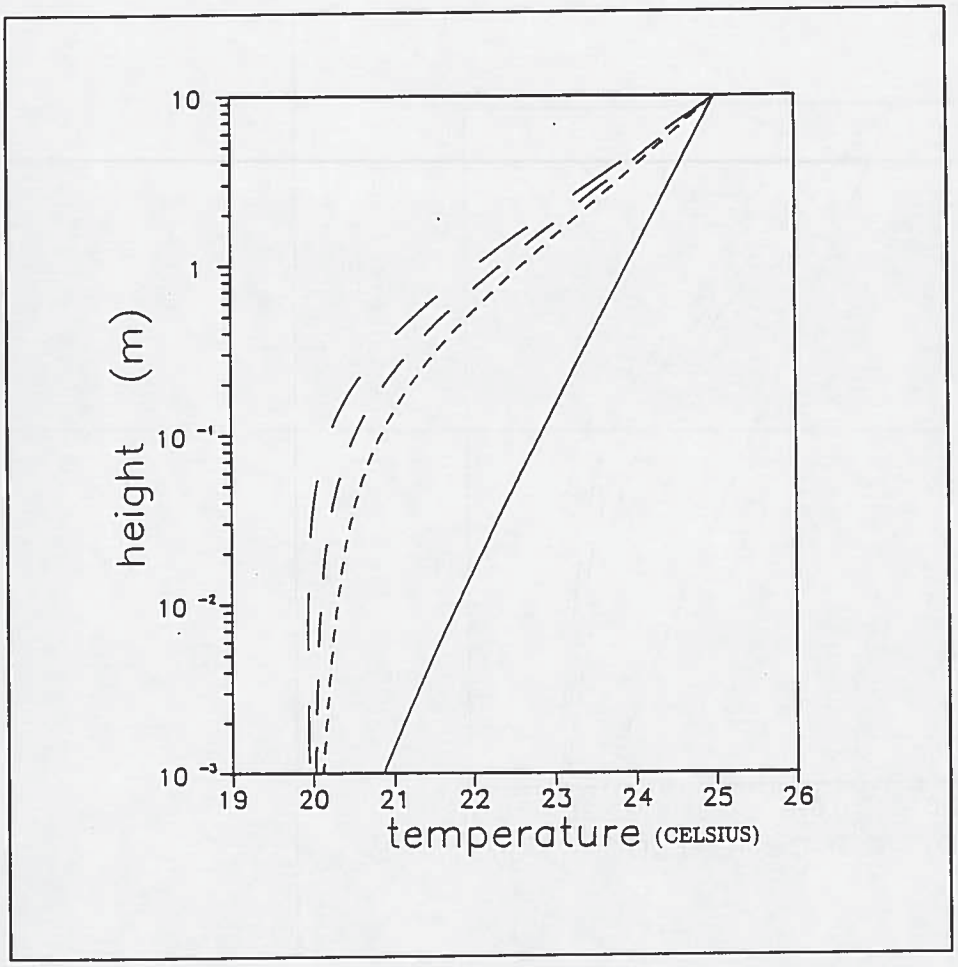

Figure 25. Vertical temperature profile, $z_{sup} = 10$ m, $u_* = 0.54$ m/s, the non-evaporative case: ———. $T_{surf} = 20°C$, $\rho_v(z_{inf}) = 0.0174$ kg m^3, $\rho_v(z_{sup}) = 0.0142$ kg/m^3, $T(z_{sup}) = 25°C$.
— — — : $r_m = 40$ microns
– – – – – : $r_m = 50$ microns
- - - - - - : $r_m = 60$ microns.

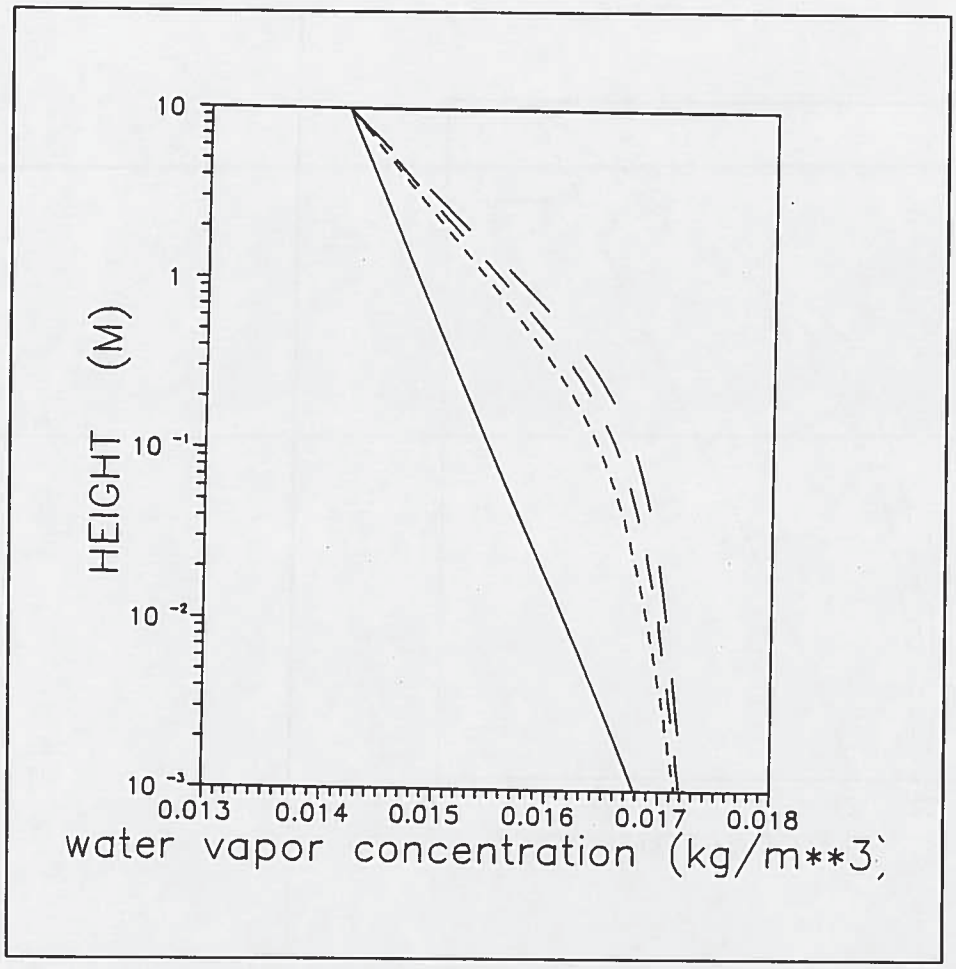

Figure 26. Vertical ρ_v-profile, $z_{sup} = 10\ m$, $u_* = 0.54\ m/s$, the non-evaporative case: ———. The evaporative case: $T_{surf} = 20°C$, $\rho_v(z_{inf}) = 0.0174\ kg\ m^3$, $\rho_v(z_{sup}) = 0.0142\ kg/m^3$, $T(z_{sup}) = 25°C$.
— — — : $r_m = 40$ microns
- - - - - : $r_m = 50$ microns
- - - - - - : $r_m = 60$ microns.

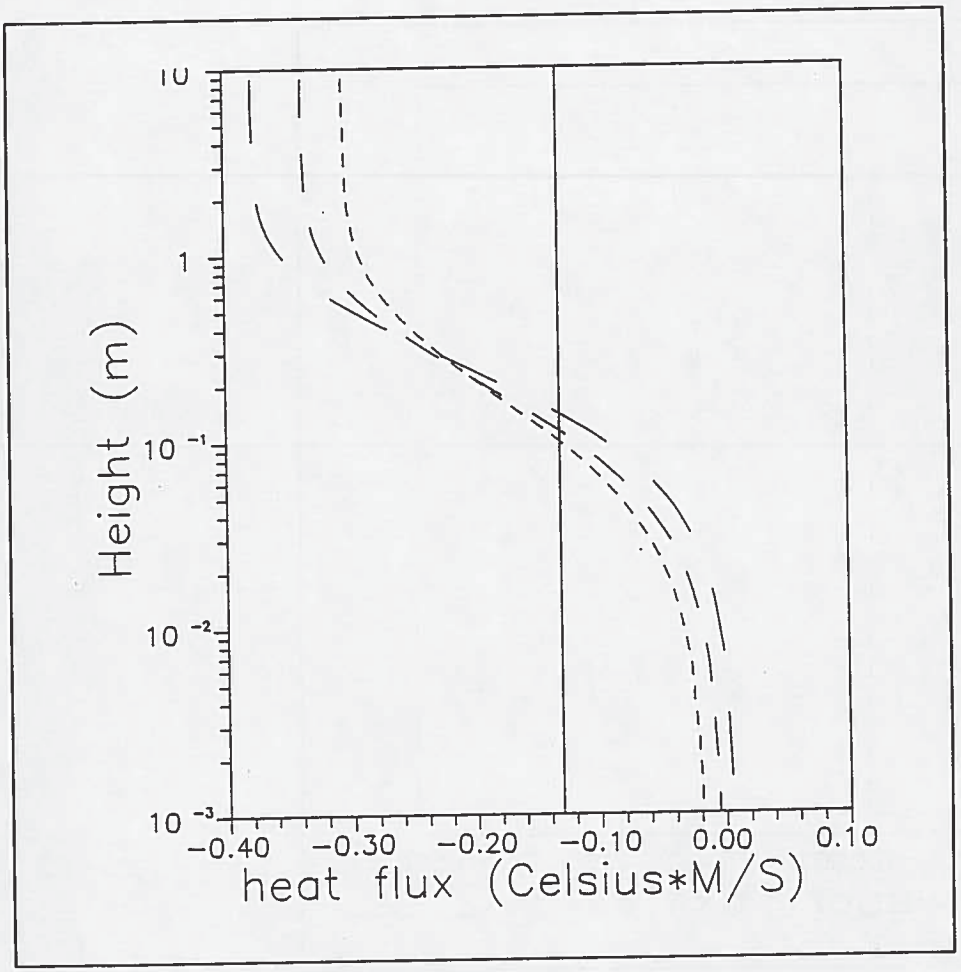

Figure 27. Vertical heat flux, $z_{sup} = 10\ m$, $u_* = 0.54\ m/s$, *the non-evaporative case:* ———. *The evaporative case:* $T_{surf} = 20°\,C$, $\rho_v(z_{inf}) = 0.0174\ kg\ m^3$, $\rho_v(z_{sup}) = 0.0142\ kg/m^3$, $T(z_{sup}) = 25°\,C$.
— — — : $r_m = 40$ microns
- - - - - : $r_m = 50$ microns
- - - - - - : $r_m = 60$ microns.

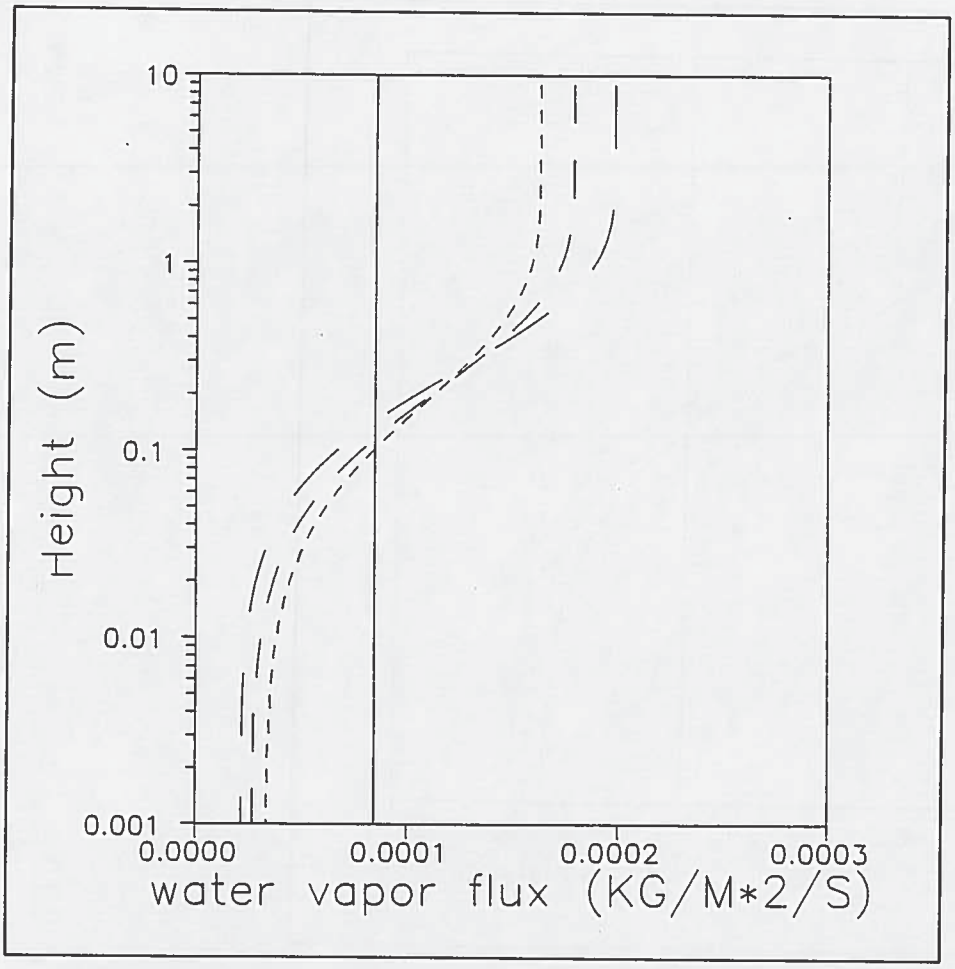

Figure 28. Vertical ρ_v-flux, $z_{sup} = 10$ m, $u_* = 0.54$ m/s, the non-evaporative case: ———. *The evaporative case:* $T_{surf} = 20°C$, $\rho_v(z_{inf}) = 0.0174$ kg m^3, $\rho_v(z_{sup}) = 0.0142$ kg/m^3, $T(z_{sup}) = 25°C$.
— — — : $r_m = 40$ microns
- - - - - : $r_m = 50$ microns
- - - - - - : $r_m = 60$ microns.

A Jet droplets in still air under non-evaporative conditions

A.1 Aim of the study

The motion of liquid in the form of droplets in still air is a simple case which can provide useful information and data in the absence of results in the turbulent case: ejection velocity from the water surface, final fall velocity (velocity when the droplet hits the surface), flight times, and vertical concentration profiles. We will use these droplet values in the turbulent model for boundary conditions or to model some terms.

A.2 Equation of motion in still air

When there is no horizontal velocity and no mass variation by evaporation, the equation of motion of a droplet in still air is given by

$$\begin{aligned} \frac{dw}{dt} &= -\frac{3}{4} Cd \frac{\rho_a}{\rho_w} \frac{w\,|w|}{2.r} - g \\ \frac{dh}{dt} &= w \end{aligned} \tag{98}$$

where

ρ_w	=	the water density
ρ_a	=	the air density
g	=	the gravitational acceleration
r	=	the droplet radius and
w	=	the vertical droplet velocity
Cd	=	the drag coefficient of a spherical droplet.

Cd a is function of the Reynolds number $\mathrm{Re} = \frac{2\,|w|\,r}{\nu}$ where ν is the cinematic air viscosity. The value of Cd is given by Raudviki (1976):

$$\begin{aligned} Cd &= 24/\mathrm{Re} && \text{if} \mathrm{Re} < 0.5 \\ Cd &= 24(1 + 0.19\,\mathrm{Re})/\mathrm{Re} && \text{if} 0.5 < \mathrm{Re} < 2 \\ Cd &= 24(1 + 0.15\,\mathrm{Re}^{0.687})/\mathrm{Re} && \text{if} 2 < \mathrm{Re} \end{aligned} \tag{99}$$

Using Eqs. (98) and (99) we can calculate numerically the droplet velocity along its trajectory, using the Runge-Kutta fourth-order method. But this method requires the initial z and w values; however, we don't know the initial value, w which is the ejection velocity. The height ejection is more easily known by measurements (1 to 20 cm for jet droplets), so we will use the ejection height mesured by Blanchard Blanchard (1963) and presented in Fig. 29 to deduce the ejection velocity by associating the Runge-Kutta method with the Newtonian method which gives the so-called "shooting method".

We begin the calculation with the Runge-Kutta method for two random values of the initial velocity; then we can calculate two maximum heights of the trajectory that we compare with the ejection height given by Blanchard (1963). Using these two values we then produce by the Newtonian method a corrected initial velocity which by the Runge-Kutta method is used again to calculate the trajectory. By iteration we can calculate the initial velocity which gives the ejection height as a maximum of the trajectory.

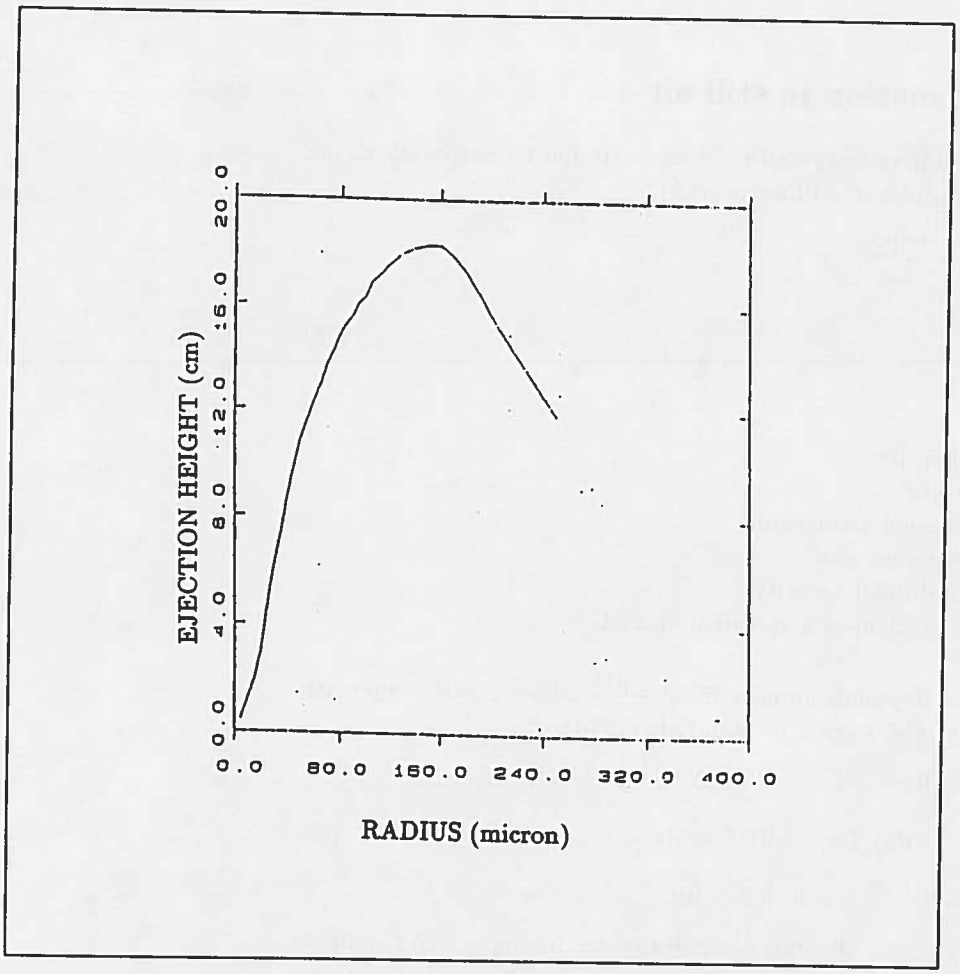

Figure 29. Ejections heights in function of the upper jet droplet radius.

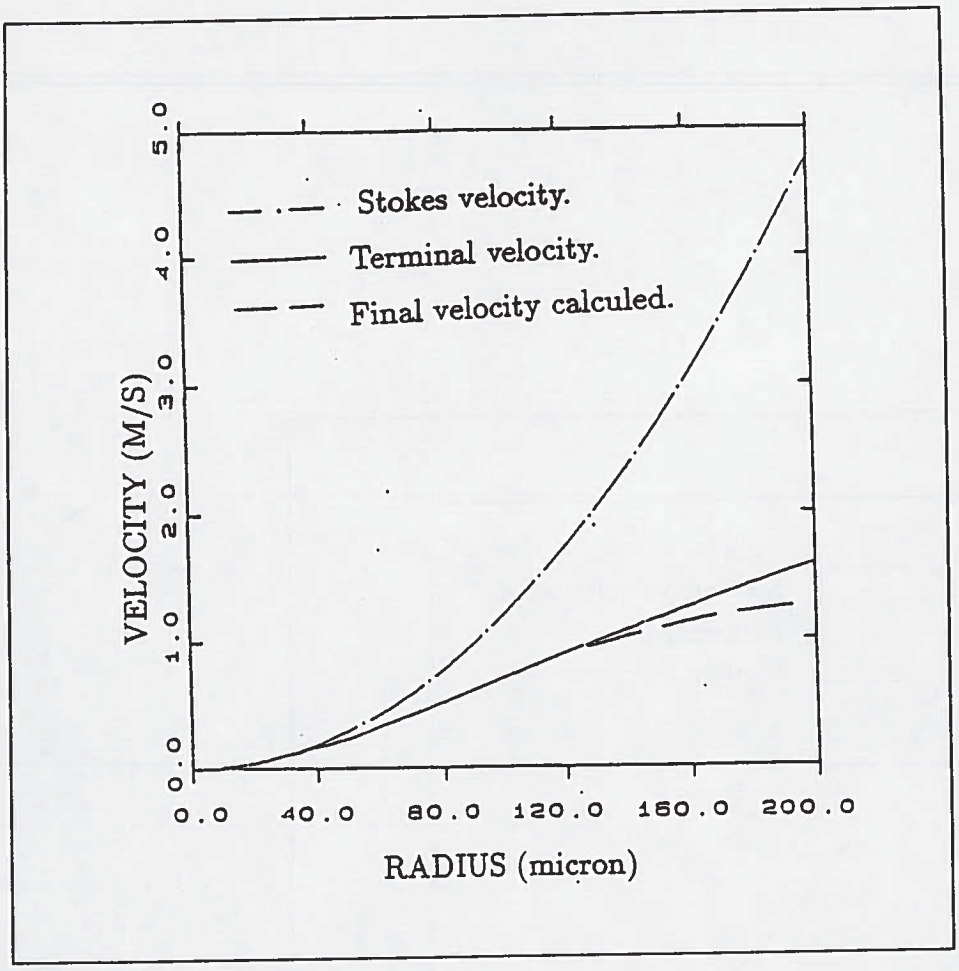

Figure 30. Fall velocity calculated (- - -) compared to Stokes and terminal velocity (—) in function of the droplet radius.

A.3 Results

This initial velocity is the ejection velocity looked for. It is compared with the ejection velocity calculated by Blanchard (1963) for jet droplets in Fig. 30. The discrepancy comes from the different drag coefficient used in the two calculations. In each we can see a discontinuity of around 10 μm in radius.

We can now calculate the droplet velocity along its trajectory, and the velocity when hitting the surface. This final fall velocity,V_f, is compared with the terminal velocity and the Stokes velocity, V_s, in Fig. 31. The terminal velocity, V_t, of a particle is given by:

$$Cd\,V_t^2 = \frac{4}{3}\,\frac{\rho_a}{\rho_w}\,2\,r\,g \tag{100}$$

which corresponds to $dw/dt = 0$ in Eq. (98), and Cd is given by Eq. (99).

The Stokes velocity, V_s, is the terminal velocity of small particles when Re<0.5 and $Cd = 24/\mathrm{Re}$. In this case Eq. (98) becomes:

$$V_s = \frac{2}{9}\,\frac{\rho_a}{\rho_w}\,\frac{g.r^2}{\nu} \tag{101}$$

If $r < 50$ μm , V_s is a good approximation of the final velocity, and the terminal velocity is a good approximation of the final fall velocity for jet droplets. From the trajectory calculation we can deduce the rise time, the downward and flight

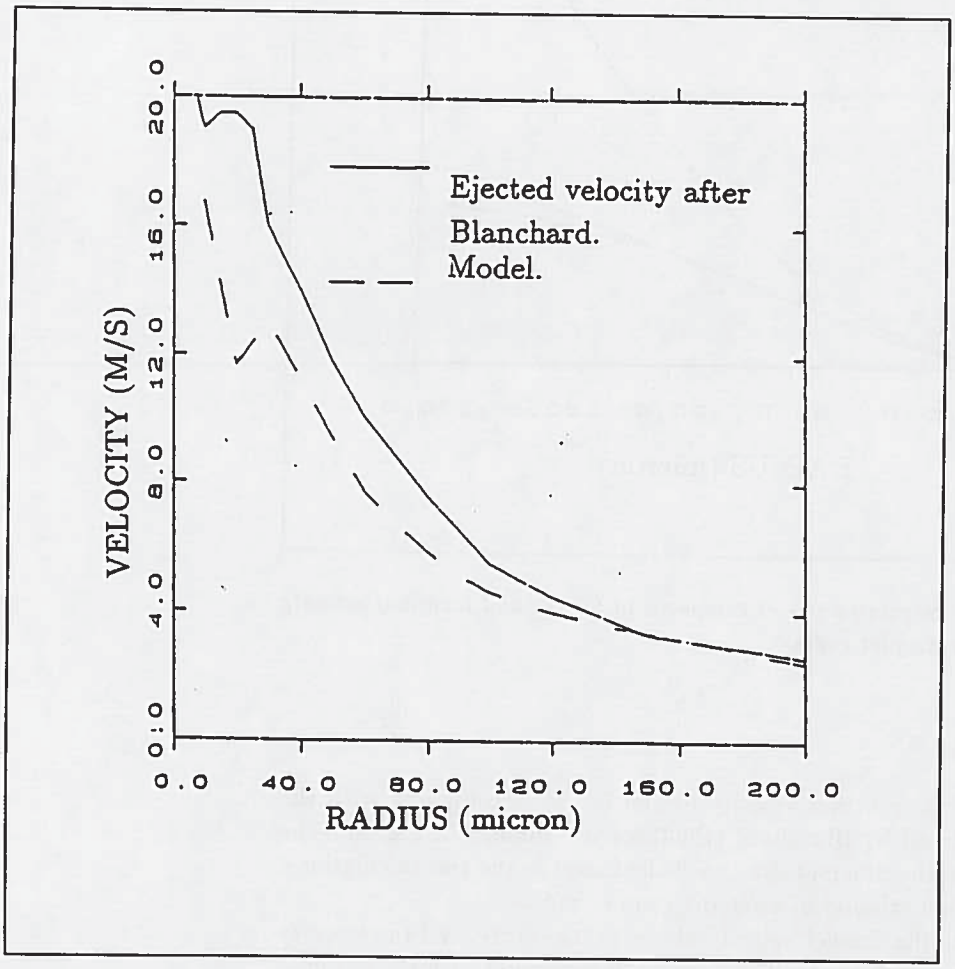

Figure 31. Ejection velocity in function of the droplet radius.

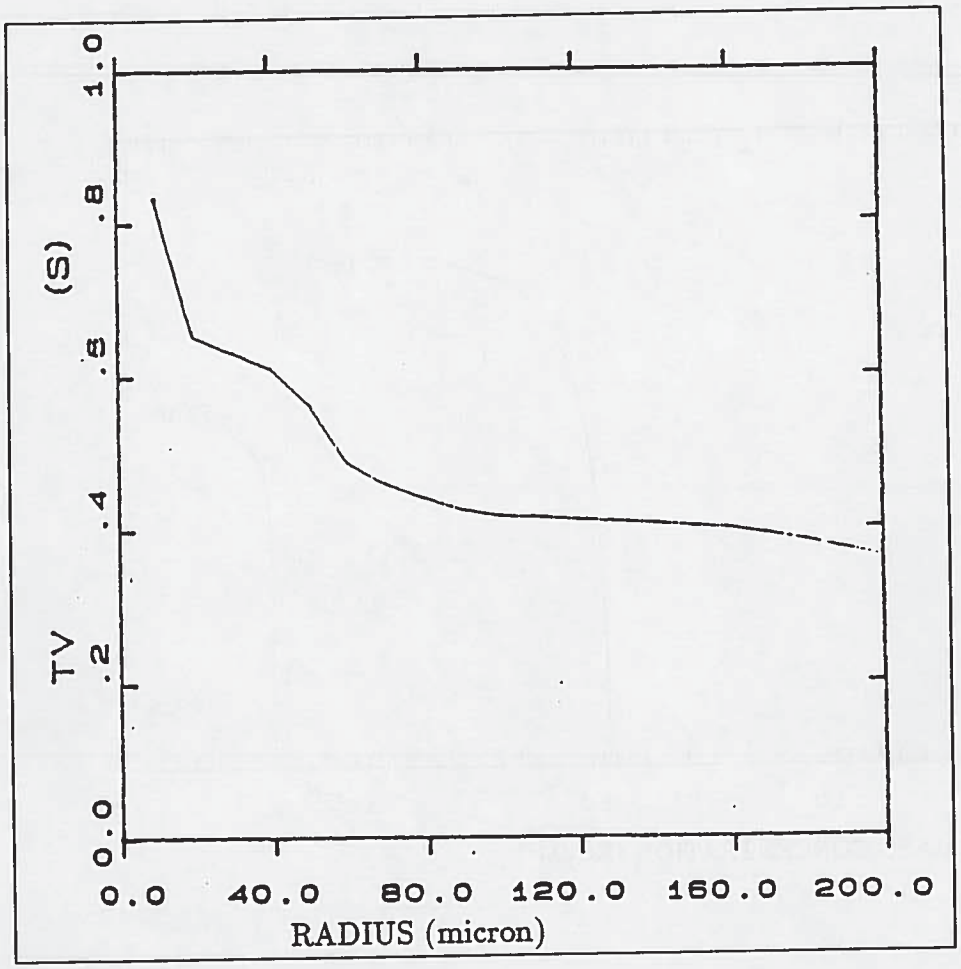

Figure 32. Suspension or flight time from the ejection to the water surface.

time which are the total suspension time. These different times are presented in Fig. 32.

We can also calculate the vertical concentration profile of droplets, ρ_{on}, from the values of droplet velocity along its trajectory and from ρ_{ne} the mass concentration of the jet dropletlets ejected by bursting of the bubbles. The ejected mass concentration of category n is defined by its radius r_n:

$$r_n - \delta_{r_n}/2 < r < r_n + \delta_{rn}/2 \tag{102}$$

and given by:

$$\rho_{ne} = dN/dr \left(\frac{4}{3}\pi \rho_w r_n^3\right) \delta_{rn} \tag{103}$$

where dN/dr is the number of ejected droplets per radius increment and per unit of volume; δ_{rn} is the radius increment of category n and r_n the nominal radius of the category n. At each height z in a small field surrounding z we can separate the concentration of category n, ρ_n, in upward concentration,ρ_{n+},with positive velocity, w_{n+}, and downward concentration ρ_{n-} with negative velocity, w_{n-}.

$$\rho_{on} = \rho_{n+} + \rho_{n-} \tag{104}$$

Under nonturbulent and non-evaporative conditions, the momentum is conserved at each height z:

$$\rho_{n+}\, w_{n+} = \rho_{n-}\, w_{n-} = \rho_{ne}\, w_{ne} \tag{105}$$

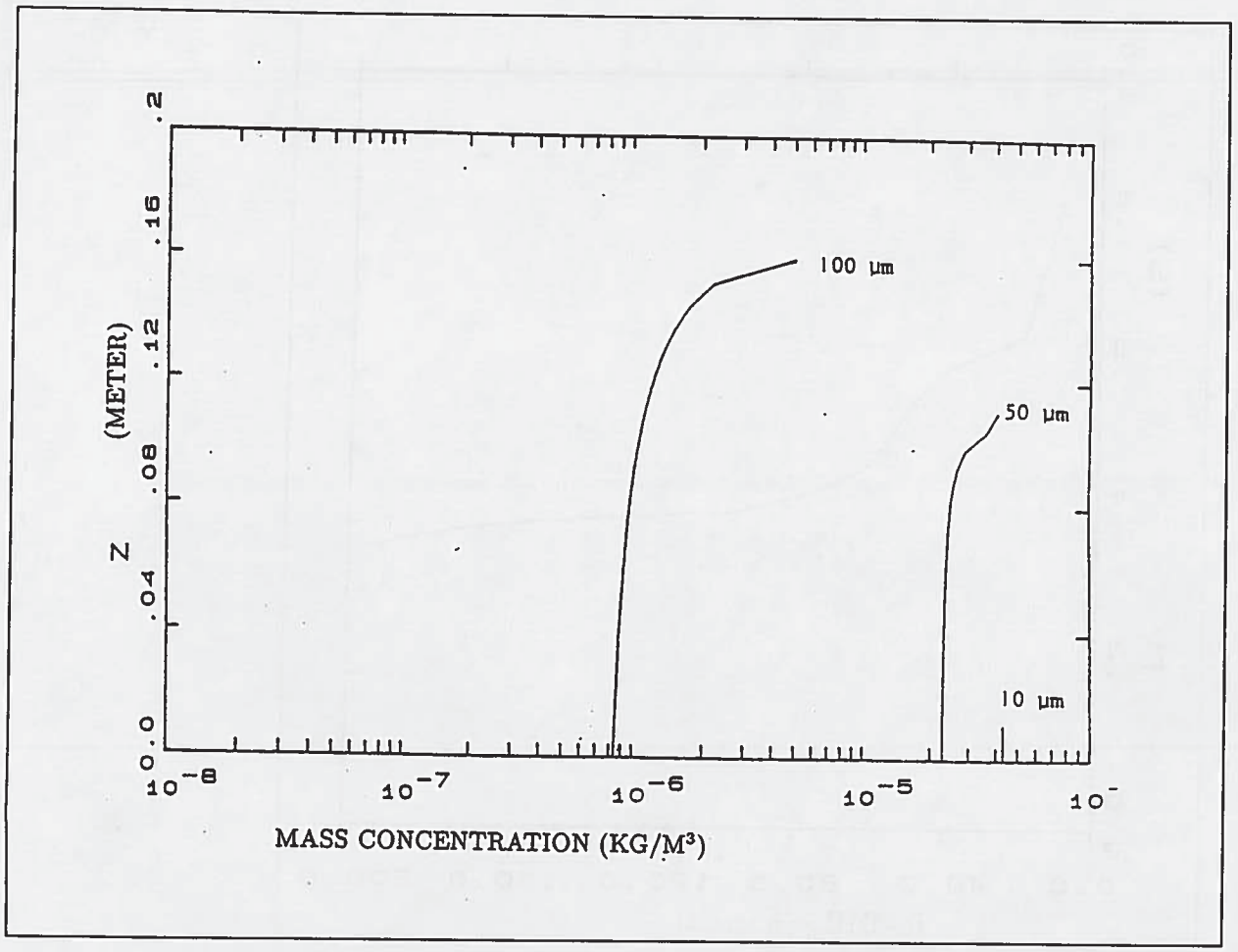

Figure 33. Mass concentration verticasl profiles ρ_{on} in non-turbulent conditions interpoalted to the grid defined in section 2.2.1.

where w_{ne} is the ejection velocity and ρ_{ne} the ejected concentration, and $\rho_{ne}\, w_{ne}$ is the ejected flux at the water surface:

$$\rho_{on} = \rho_{ne}\, w_{ne} \left(\frac{1}{w_{n+}} + \frac{1}{w_{n-}} \right) \tag{105}$$

Figure 33 presents three vertical mass profiles for three categories (n = 1, 5, 10), $r_1 = 10\ \mu$m, $r_5 = 5\ \mu$m, $r_{10} = 100\ \mu$m, $\delta_{r_n} = 10\ \mu$m for all categories. $\rho_{e1} = 5.10^{-8}\ kg/m^3$, $\rho_{e2} = 140.10^{-8}\ kg/m^3$, $\rho_{e10} = 9.10^{-8}\ kg/m^3$.

Because these results are interpolated to the CLUSE model grid (section 2.2.1) the top of each curve have a different shape: the ejection heights do not correspond to the top of each integration domain. We assume that one bubble gives one jet droplet rising to the maximum ejection height given by Blanchard (1963).

We see that we can approximate theses profiles assuming that the drops appear at their ejection height and have immediately their final velocity. Thus these profile can be described by:

$$\rho_{on} = \frac{\rho_{ne}\, w_{ne}}{V_l} \tag{106}$$

Acknowledgements

To a large extent this report is built on the PH.D. thesis of the first author: Modelisation Numerique d'une couche limite Unidimensionelle Stationnaire d'Embruns. The authors wish to acknowledge many discussions with the primary advisers of this project, P.G. Mestayer and R. Shiestel. Furthermore, the report utilizes data obtained during the 1988 CLUSE and the 1985 HEXIST experiment in the air-water tunnel at the I.MS.T. luminy facility. The participants in this experiment are gratefully acknowledged both for use of the experimental data for model calibration and for many stimulating discussions, notably J.B. Edson, C.W. Fairall, G. de Leeuw and E.C. Monahan. The work with this report has been supported by the Danish HAV90 experiment under project 4–01.

References

ANDREAS L.,E. (1989). Thermal and size evolution of sea spray droplets. CRREL Report 89-11. U.S. Army Cold Regions Research and Engineering Laboratory, Hannover, N.H., USA.

BEARD K.V. and H.R. PRUPACHER (1971). A wind tunnel investigation of rate of evaporation of small water drops failling at terminal velocity in air. *J.Atmos.Sci.*, **28**, 1455–1464.

BLANCHARD D.C. (1963). Electrification of the atmosphere by particles from bubbles in the sea. Progress in Oceanography, 1, Pergamon Press, 73–202.

BORTKOVSKII,R.S. 1987). Air-sea Exchange of heat and moisture during storms, D.Reidel Publ. Co., Dordrecht, xiii + 194 pp.

BUCK,A.L., (1981). New equations for computing vapor pressure and enhancement factor. *J. Appl. Meteor.*, **20**, 1527–1532.

DE LEEUW G. (1988. Survey of the CLUSE main experiment GRAND-CLUSE. Physics and Electronics Lab. TNO Report.

EDSON J.B. (1987). Lagrangian model simulation of the turbulent transport and evaporation of spray droplets in a wind–water tunnel. M.S. Thesis, Department of Meteorology,Pennsylvania State University, University Park, PA, USA (not published).

EDSON J. (1989). Lagrangian model simulation of the turbulent transport of evaporating jet droplets. Ph.D. thesis, Dept. of Meteorology, Penn State University, PA, USA.

LING S.C., T.W. KAO, M.ASCE and A.SAAD (1980). Microdoplets and transport of moisture from the ocean. *J.Eng.Mech.Div.*, **6**, 1327–1339.

MELVILLE W.K. and K.N.C. BRAY (1979). A model of the two-phase turbulent jet. *Int. J. Heat Mass Transfert*, **22**, 647–656.

PATANKAR S.V. and D.B.SPALDING (1970). Heat and mass transfert in boundary layers: a general calculation procedure, 2nd ed., Intertext Book, London.

PRUPACHER H.R. and J.D. KLETT (1978). Microphysics of clouds and precipitation, Reidel, Dordrecht, Holland.

RAUDVIKI A.J. (1976). Loose Boundary Hydraulics, 2nd ed., Pergamon Press, New–York.

ROUAULT M. (1989). Modelisation numerique d'une couche limite unidimensionelle stationnaire d'embruns. These de doctorat, Université d'aix-Marseille 2.

Bibliographic Data Sheet **Risø-M-2847**

Title and author(s)

Spray droplets under turbulent conditions

Mathieu Rouault and Søren E. Larsen

ISBN
87-550-1608-1

ISSN
0418-6435

Dept. or group
Meteorology and Wind Energy

Date
January 1990

Groups own reg. number(s)

Project/contract no.

Pages	Tables	Illustrations	References
60	0	33	14

Abstract (Max. 2000 char.)

In the frame of the international cooperative program HEXIST, in parallel to the experiments conducted in IMST Large Air-Sea Interaction Simulation Tunnel, we have developed a numerical model of turbulent transport and evaporation of a population of droplets ejected by bursting bubbles at the water surface. This numerical model considers fresh water droplets from 10 to 100 microns radius (jet drops), in a fully developed turbulent boundary layer or any constant flux layer, with no surface waves. The droplet population is separated in 20 categories according to their size, and each category is considered as a scalar field transported along with the scalar fields of temperature and water vapor concentration by turbulence. Theses fields are interacting through source-sink functions, representing droplets shrinking and water vapour production due to droplet evaporation. Droplet surface production and deposition processes, and inertial and gravitational effects are explicitly modeled. Droplet diffusion by air turbulence is modeled by a K diffusivity. The model has been fitted to the conditions of CLUSE-HEXIST 3, the large experiment that has been conducted by HEXIST participants in the IMST tunnel in May-June 1988.

After a description of the model and numerical method we will make some comparisons with the experiment CLUSE-HEXIST 3. Then we will study some cases in a idealistic constant flux boundary layer in different humidity and wind configurations. Finally, we will compare our ejected drop flux to that found by Bortkovskii (1987) which will be used in different configurations.

Descriptors INIS/EDB

Available on request from:
Risø Library, Risø National Laboratory (Risø Bibliotek, Forskningscenter Risø)
P.O. Box 49, DK-4000 Roskilde, Denmark
Phone +45 42 37 12 12, ext. 2268/2269 · Telex 43 116 · Telefax +45 46 75 56 27

Available on exchange from:
Risø Library,
Risø National Laboratory, P.O. Box 49,
DK-4000 Roskilde, Denmark
Phone +45 42 37 12 12, ext. 2268/2269
Telex 43 116, Telefax +45 46 75 56 27

ISBN 87-550-1608-1
ISSN 0418-6435